EUROPEAN ORGANIZATION FOR NUCLEAR RESEARCH

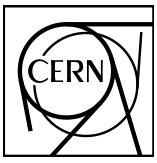

CERN-EP-2023-194
30 August 2023

Dielectron production in central Pb–Pb collisions at $\sqrt{s_{\rm NN}} = 5.02$ TeV

ALICE Collaboration*

arXiv:2308.16704v1 [nucl-ex] 31 Aug 2023

Abstract

The first measurement of the e^+e^- pair production at midrapidity and low invariant mass in central Pb–Pb collisions at $\sqrt{s_{\rm NN}} = 5.02$ TeV at the LHC is presented. The yield of e^+e^- pairs is compared with a cocktail of expected hadronic decay contributions in the invariant mass ($m_{\rm ee}$) and pair transverse momentum ($p_{\rm T,ee}$) ranges $m_{\rm ee} < 3.5$ GeV/c^2 and $p_{\rm T,ee} < 8$ GeV/c. For $0.18 < m_{\rm ee} < 0.5$ GeV/c^2 the ratio of data to the cocktail of hadronic contributions without ρ mesons amounts to 1.42 ± 0.12 (stat.) ± 0.17 (syst.) ± 0.12 (cocktail) and 1.44 ± 0.12 (stat.) ± 0.17 (syst.) $^{+0.17}_{-0.21}$ (cocktail), including or not including medium effects in the estimation of the heavy-flavor background, respectively. It is consistent with predictions from two different models for an additional contribution of thermal e^+e^- pairs from the hadronic and partonic phases. In the intermediate-mass range ($1.2 < m_{\rm ee} < 2.6$ GeV/c^2), the pair transverse impact parameter of the e^+e^- pairs ($\rm DCA_{ee}$) is used for the first time in Pb–Pb collisions to separate displaced dielectrons from heavy-flavor hadron decays from a possible (thermal) contribution produced at the interaction point. The data are consistent with a suppression of e^+e^- pairs from $c\bar{c}$ and an additional prompt component. Finally, the first direct-photon measurement in the 10% most central Pb–Pb collisions at $\sqrt{s_{\rm NN}} = 5.02$ TeV is reported via the study of virtual direct photons in the transverse momentum range $1 < p_{\rm T} < 5$ GeV/c. A model including prompt photons, as well as photons from the pre-equilibrium and fluid-dynamic phases, can reproduce the result, while being at the upper edge of the data uncertainties.

© 2023 CERN for the benefit of the ALICE Collaboration.
Reproduction of this article or parts of it is allowed as specified in the CC-BY-4.0 license.

*See Appendix A for the list of collaboration members

1 Introduction

Ultra-relativistic heavy-ion collisions at the Large Hadron Collider (LHC) allow the study of strongly interacting matter at high temperature and small net-baryon density [1]. Under these conditions, the theory of the strong interaction, quantum chromodynamics (QCD), predicts a transition from ordinary matter made of hadrons to a quark–gluon plasma (QGP) in which quarks and gluons are deconfined [2–5]. In this QGP phase, chiral symmetry is also expected to be restored [6, 7]. Photons and dileptons, i.e. lepton–antilepton pairs originating from the internal conversion of virtual photons, are produced at all stages of the heavy-ion collision with negligible final-state interactions, unlike hadrons. Therefore, they carry undistorted information about the whole space–time evolution of the medium created in such collisions.

Direct photons are photons not originating from hadronic decays. They are emitted by various sources as discussed in Ref. [8]. Prompt direct photons are produced in the initial hard parton–parton scatterings. Additional photons, still generated before the system reaches sufficient equilibrium to be described by relativistic viscous hydrodynamics, are called pre-equilibrium photons. Thermal photons are emitted from the deconfined QGP and hot hadronic matter and are characterized by the thermal distributions of partons and hadrons, respectively. Other direct photon production mechanisms are not excluded, like the interaction of hard-scattered partons from jets with the plasma [9, 10]. Each source of direct photons populates different transverse momentum ($p_{\rm T}$) regions. Prompt direct photons follow a power-law spectrum and dominate at high $p_{\rm T}$ ($p_{\rm T} \gtrsim 5$ GeV/c). At lower $p_{\rm T}$ ($p_{\rm T} \lesssim 2$ GeV/c), thermal photons are expected to contribute significantly with an approximately exponential $p_{\rm T}$ spectrum containing information on the initial temperature and space–time evolution of the medium [11, 12]. Pre-equilibrium photons may play a role in the intermediate $p_{\rm T}$ range [13].

The first measurement of a direct photon signal in relativistic heavy-ion collisions was reported by the WA98 collaboration [14] in central Pb–Pb collisions at the center-of-mass energy per nucleon pair $\sqrt{s_{\rm NN}} = 17.3$ GeV. The spectrum is consistent with calculations for thermal photon radiation from a quark–gluon plasma and a hot hadronic phase, as well as with predictions including multiple soft scatterings of the incoming partons without the formation of a QGP [12]. At the Relativistic Heavy Ion Collider (RHIC), the first $p_{\rm T}$-differential yield of direct photons was measured by the PHENIX collaboration in Au–Au collisions at $\sqrt{s_{\rm NN}} = 0.2$ TeV [15], followed by subsequent results at the same center-of-mass energy per nucleon pair [16–20] as well as at lower energies [21, 22]. On the one hand, the measured direct-photon yields are well described by the expected yields of prompt direct photons at high $p_{\rm T}$ ($p_{\rm T} \gtrsim 5$ GeV/c), showing that the high-$p_{\rm T}$ direct photons are predominantly from initial hard-scattering processes. The prompt component is estimated either from measurements in pp and d–Au collisions at the same collision energy [23–25] or perturbative QCD calculations [26], both scaled with the number of binary nucleon–nucleon collisions ($N_{\rm coll}$). On the other hand, a large excess of direct photons is observed at low $p_{\rm T}$ ($p_{\rm T} < 2$ GeV/c) with respect to the expected prompt direct photon yields. The STAR collaboration also reported an enhancement of direct photons at low $p_{\rm T}$ in Au–Au collisions at $\sqrt{s_{\rm NN}} = 0.2$ TeV [27], which appears to be about a factor three smaller than the one measured by PHENIX. The large yield of direct photons is accompanied by a large azimuthal anisotropy (elliptic flow) with respect to the reaction plane [17, 20], similar in magnitude to the one of charged hadrons, suggesting a large contribution from the late stages of the collision. A simultaneous description of the $p_{\rm T}$-differential yields and elliptic flow results remains challenging for models [13, 28–31]. At the LHC, direct photon yield [32] and elliptic flow [33] measurements in Pb–Pb collisions at $\sqrt{s_{\rm NN}} = 2.76$ TeV by the ALICE collaboration show similar trends as those from PHENIX within the experimental uncertainties. Recent results by the PHENIX collaboration, obtained with a factor ten larger dataset of Au–Au collisions at $\sqrt{s_{\rm NN}} = 0.2$ TeV, reduce the tension between the measured direct-photon yield in central Au–Au collisions [19] and the predictions from a state-of-the-art model [13] including prompt, pre-equilibrium, and thermal photons. The observed direct-photon yields in more peripheral Au–Au col-

lisions remain nevertheless a factor two to three larger than the calculations. Effective temperatures ($T_{\rm eff}$) were extracted from the measured $p_{\rm T}$ spectra at low $p_{\rm T}$ in Au–Au collisions at $\sqrt{s_{\rm NN}} = 0.2$ TeV [19] and in Pb–Pb collisions at $\sqrt{s_{\rm NN}} = 2.76$ TeV [32] by the PHENIX and ALICE collaborations, respectively. The measured $T_{\rm eff}$ values are significantly larger than the critical temperature for chiral symmetry restoration and color deconfinement. This does not prove that the radiation is emitted from a QGP, since radiation from the late stages of the collision with strong radial flow could lead to a significant blue shift. Detailed studies of the direct-photon yield as a function of the collision system size by PHENIX show a power-law dependence on the charged-particle multiplicity at midrapidity ($\frac{{\rm d}N_{\rm ch}}{{\rm d}\eta}|_{\eta=0}$) at low $p_{\rm T}$. The measured power α seems to have a weak dependence on centrality or collision energy [21, 22] and no apparent dependence on $p_{\rm T}$, in particular in Au–Au collisions at $\sqrt{s_{\rm NN}} = 0.2$ TeV [19]. However, model calculations predict different α for radiation from different phases [34].

In contrast to real photons, virtual photons, i.e. dileptons, carry a mass, the invariant mass of the lepton and antilepton pair ($m_{\rm l^+l^-}$). This provides an additional means to disentangle the different sources of electromagnetic radiation. For $m_{\rm l^+l^-} > 1.2$ GeV$/c^2$, virtual direct photons are foreseen to originate from the partonic phase of the heavy-ion collision [35]. In the mass region $1.2 < m_{\rm l^+l^-} < 2.6$ GeV$/c^2$ thermal radiation from the QGP is expected to contribute significantly to the virtual direct-photon yield [36]. The slope of their $m_{\rm l^+l^-}$ distribution is predicted to carry information about the early temperature in the medium without distortion due to blueshift effect [35]. Nevertheless, correlated background from semileptonic decays of open heavy-flavor hadrons has to be subtracted or rejected first. Moreover, initial hard parton–parton scatterings generate also direct dileptons via the Drell-Yan process. While this process contributes significantly to the measured dilepton spectra down to small invariant masses ($m_{\rm l^+l^-} \approx 1.5$ GeV$/c^2$) at SPS energies, it is estimated to be negligible for masses up to about 3 GeV$/c^2$ at the LHC. On the other hand, recent theoretical calculations for Pb–Pb collisions at $\sqrt{s_{\rm NN}} = 5.02$ TeV show that additional $\rm l^+l^-$ pairs, still produced before the system reaches local thermal equilibrium, may play a role for $m_{\rm l^+l^-} > 1.5$ GeV$/c^2$ [37, 38]. At lower $m_{\rm l^+l^-}$ ($m_{\rm l^+l^-} < 1.2$ GeV$/c^2$), the dilepton invariant mass can be used to study the decay of massive particles, such as the in-medium modified spectral shape of vector mesons. Dileptons produced in the medium in the vicinity of the transition temperatures are sensitive to effects related to chiral symmetry restoration [39, 40]. Due to its strong coupling to the $\pi^+\pi^-$ channel and its life time of only 1.3 fm$/c$, much smaller than that of the fireball at the LHC (≈ 10 fm$/c$), the ρ meson is expected to be the most sensitive to such medium effects. Finally, in the zero mass limit, the fraction of virtual direct photons over inclusive virtual photons is expected to be identical to that of real photons [41]. Therefore the measured dilepton yield in the quasi-real virtual-photon region, where the pair transverse momenta $p_{\rm T,ll}$ is much larger than $m_{\rm l^+l^-}$, can be used to measure the $p_{\rm T}$-differential yield of direct photons.

Precision measurements of virtual photons were performed at the CERN SPS by the CERES [42–44] and NA60 [45–48] collaborations in the dielectron and dimuon channels, respectively. An average temperature of about 200 MeV, significantly above the transition temperatures, was extracted from the mass spectrum in $1.2 < m_{\rm l^+l^-} < 2$ GeV$/c^2$ in 158A GeV In–In collisions by the NA60 collaboration [48]. The capability of the NA60 experiment to disentangle prompt muons, originating from the primary vertex, and non-prompt muons from displaced open-charm hadron decays, allowed them to explicitly attribute the observed dimuon signal in this mass range to a prompt source. Together with studies of the effective temperature $T_{\rm eff}$ from the dimuon $p_{\rm T}$ spectrum as a function of mass [47], this temperature value suggested that dilepton radiation in the intermediate-mass region originates from the partonic phase [49, 50]. For increasing $\sqrt{s_{\rm NN}}$, the correlated background from heavy-flavor hadron decays becomes very large with respect to the QGP radiation, preventing the PHENIX [51], STAR [52], and ALICE [53] collaborations at RHIC and the LHC from extracting an unambiguous dilepton signal in the intermediate-mass range without the use of high-precision vertex detectors. At lower mass, the ρ properties in the hot medium created in heavy-ion collisions were measured by the CERES and NA60 collaboration at SPS energies. The dilepton excess, obtained after subtraction of the expected contribution of other light-flavor

meson decays happening at a later stage in the collision, was found to be well described by the calculations of a microscopic many-body model [54, 55]. This model predicted a very strong broadening of the ρ spectral function with essentially no mass shift, consistent with chiral symmetry restoration [40]. At the top RHIC energy, an enhancement of dileptons in the low-mass region was reported by both the STAR [52] and the PHENIX [51] collaborations in central Au–Au collisions at $\sqrt{s_{\rm NN}} = 0.2$ TeV. Models reproducing the SPS data and involving the broadening of the ρ meson [56, 57] were shown to describe the RHIC data as well. The first low-mass dilepton results at the LHC, published by the ALICE collaboration in central Pb–Pb collisions at $\sqrt{s_{\rm NN}} = 2.76$ TeV [53], are in line with the expectations from these models, although no significant excess was observed within the limited precision of the data.

Measurements of direct photons and dileptons at LHC energies could shed light on the remaining discrepancy between those results and theory predictions. Heavy-ion collisions at the LHC provide nowadays the highest-temperature and longest-lived experimentally accessible QGP. Therefore, the thermal radiation yield is expected to be the largest with respect to measurements at other accelerator facilities. Moreover, the in-medium modifications of vector mesons can be probed under conditions that are most closely related to the regime accessible by lattice QCD (vanishing net-baryon density). However, the large combinatorial and heavy-flavor backgrounds pose a serious challenge.

In this article, the first dielectron and resulting direct-photon measurements in the 10% most central Pb–Pb collisions at $\sqrt{s_{\rm NN}} = 5.02$ TeV are presented and compared to measurements at lower energies (RHIC and LHC) and with model predictions. The uncertainties could be reduced compared to the previous publication in central Pb–Pb collisions at lower energy [53] due to the three times larger data sample. While direct photons have already been measured in central collisions at $\sqrt{s_{\rm NN}} = 2.76$ TeV as part of a real-photon analysis [32, 33], a direct-photon measurement is now available for the first time at the highest collision energy. Finally, the larger data sample allows for the first studies in Pb–Pb collisions of a topological separation of prompt dielectrons and dielectrons originating from displaced correlated heavy-flavor hadron decays. The article is organized as follows. Section 2 contains a brief description of the ALICE apparatus and the used data sample. Section 3 illustrates the data analysis techniques. Section 4 explains how the expected dielectron yields from known hadronic sources are calculated. The results are presented and discussed in Sec. 5 for the inclusive dielectron production, Sec. 6 for the topological separation of $\rm e^+e^-$ sources, and Sec. 7 for the direct-photon measurement. Finally, they are summarized in Sec. 8.

2 Detector and data sample

A detailed description of the ALICE apparatus and its performance can be found in Refs. [58, 59]. The main detectors used for the track reconstruction and electron identification at midrapidity ($|\eta| < 0.9$) are the Inner Tracking System (ITS) [60], the Time Projection Chamber (TPC) [61], and the Time-Of-Flight (TOF) detector [62]. They are located inside a large solenoidal magnet, providing a uniform magnetic field of 0.5 T parallel to the LHC beam direction. Charged-particle trajectories are reconstructed from their signals in the ITS and the TPC. The ITS consists of a six-layer silicon detector with the innermost layer installed at a radius of 3.9 cm from the beam axis. It is used for tracking, for the reconstruction of the main vertex of the collision, and for the measurement of the distance-of-closest-approach (DCA) of the track to this primary vertex. Moreover, the four outer layers, made of silicon drift detectors and silicon strip detectors, provide charged-particle identification (PID) via the measurement of their specific energy loss ($\mathrm{d}E/\mathrm{d}x$) in the detector material. The TPC, a 500 cm long gas filled cylinder providing up to 159 three-dimensional space points per track, is the main tracking detector. The measured $\mathrm{d}E/\mathrm{d}x$ of the charged particles in the gas allows electron identification over a large momentum range (up to a momentum of 10 GeV/c). The TOF detector extends at intermediate momenta ($0.4 < p < 1.3$ GeV/c) the PID capabilities of the TPC and ITS via the measurement of the time-of-flight of charged particles from the interaction point to the detector.

The data used in this article were collected by ALICE in 2018 during Pb–Pb runs at $\sqrt{s_{\rm NN}} = 5.02$ TeV. A minimum bias interaction trigger was provided by the V0 detector [63]. Simultaneous signals in the two scintillator arrays covering the pseudorapidity intervals $-3.7 < \eta < -1.7$ (V0C) and $2.8 < \eta < 5.1$ (V0A) were required. In addition, events were selected online based on the signal amplitude in these detectors in order to enrich the sample of central Pb–Pb collisions. Further selection criteria were applied later offline. Events due to the interaction of the beams with residual gas in the beam pipe were rejected using the V0 and the Zero Degree Calorimeter (ZDC) [64] timing information. Pileup collisions occurring during the TPC readout time were removed using the correlation between the number of tracks reconstructed in the TPC and in the ITS, which grants a faster readout. Only events with a primary vertex reconstructed within ± 10 cm from the center of the detector along the beam axis were considered. Finally, the 10% most central Pb–Pb collisions were defined in terms of percentiles of the hadronic Pb–Pb cross section using the sum of the V0 signal amplitudes as described in detail in Ref. [65]. The corresponding average value of the nuclear overlap function, $\langle T_{\rm AA} \rangle$, is (23.26 ± 0.17) mb^{-1} [65]. The total number of selected events ($N_{\rm events}$) is about 65×10^6 corresponding to an integrated luminosity of 85 μb^{-1} [66].

3 Data analysis

3.1 Dielectron raw yields

Electron candidates are selected in the transverse momentum range $0.2 < p_{\rm T,e} < 10$ GeV/c and at midrapidity ($|\eta_{\rm e}| < 0.8$). For the analysis using the DCA information to separate dielectrons from different sources, the tracks must have a $p_{\rm T} > 0.4$ GeV/c to assure a sufficient separation between prompt $\rm e^+e^-$ pairs originating from the primary vertex and non-prompt ones arising from displaced open heavy-flavor hadron decays. The DCA resolution worsens at low $p_{\rm T}$. For tracks reconstructed in the ITS and TPC with a transverse momentum smaller than 0.35 GeV/c the DCA resolution in the plane perpendicular to the beam axis is larger than 150 μm [67] and thus comparable to the decay length of the $\rm D^0$ and $\rm D_s^{\pm}$ mesons. The same tracking selection criteria as those described in Ref. [68] are applied. In particular, a hit in the first ITS layer is required to be attached to the reconstructed track and a maximum of one ITS cluster, not placed in the first ITS layer, may be shared with any other track candidate. These requirements reduce the amount of electron tracks originating from photon conversion in the detector material by 98.8%, keeping 93.7% of the signal electrons.

The electron identification is based on the complementary information provided by the ITS, TPC, and TOF. The detector PID signals, $n(\sigma_i^{\rm DET})$, are expressed in terms of the deviation between the measured and expected value of the specific ionization energy loss in the ITS (TPC) or time-of-flight in the TOF for a given particle hypothesis i and momentum, normalized to the respective detector resolution. Electrons are identified in a similar way as described in Ref. [68]. To increase the electron purity, an asymmetric electron selection criterium is applied in the TPC, i.e. $-2 < n(\sigma_{\rm e}^{\rm TPC}) < 3$. Kaons, protons and pions are rejected with the requirements $|n(\sigma_{\rm K}^{\rm TPC})| > 3$, $|n(\sigma_{\rm p}^{\rm TPC})| > 3$ and $n(\sigma_{\pi}^{\rm TPC}) > 3.5$, respectively. To increase the PID efficiency ($\varepsilon_{\rm PID}$) and avoid a strong momentum dependence of $\varepsilon_{\rm PID}$, the ITS and TOF are used to recover electrons with an energy loss in the TPC in the range where the charged kaon and proton bands cross the one of electrons. It exploits the fact that kaons (protons) and electrons are still separated in the energy loss measurements in the ITS or the measured time-of-flight in the TOF, at momenta where they have a very similar energy loss in the TPC. Tracks which fulfill only the TPC electron selection and pion rejection but have an associated TOF signal with $-3 < n(\sigma_{\rm e}^{\rm TOF}) < 3$ or an associated ITS signal with $n(\sigma_{\rm e}^{\rm ITS}) < 2$ not consistent with the kaon ($|n(\sigma_{\rm K}^{\rm ITS})| < 2$) or proton ($|n(\sigma_{\rm p}^{\rm ITS})| < 2$) hypothesis are accepted. The final hadron contamination in the single-electron candidate sample is estimated to be less than 3.3% integrated over $p_{\rm T}$.

A statistical approach is applied to extract the yield of correlated signal pairs (S). To this end, all electron

and positron candidates from the same event are combined into opposite-sign pairs ($N^{\rm same}_{+-}$), characterised by their invariant mass $m_{\rm ee}$, pair transverse momentum $p_{\rm T,ee}$ and pair DCA$_{\rm ee}$, similarly to the approach followed by the NA60 collaboration [69]. The latter is calculated from the single-electron DCAs as

$$\mathrm{DCA_{ee}} = \sqrt{\frac{(\mathrm{DCA}_{xy,1}/\sigma_{xy,1})^2 + (\mathrm{DCA}_{xy,2}/\sigma_{xy,2})^2}{2}}, \tag{1}$$

where DCA$_{xy,i}$ is the DCA of the electron i in the transverse plane and $\sigma_{xy,i}$ is its resolution estimated from the covariance matrix of the track reconstruction parameters obtained with the Kalman filter technique, similarly as in Ref. [70]. The combinatorial background (B) is estimated via the geometric mean of same-sign pairs from the same event $\sqrt{N^{\rm same}_{++}N^{\rm same}_{--}}$, corrected for the different acceptance for opposite-sign and same-sign pairs [53, 70]. The correction factor R is calculated using uncorrelated opposite- ($N^{\rm mix}_{+-}$) and same-sign ($N^{\rm mix}_{++}$ and $N^{\rm mix}_{--}$) pairs from mixed events with similar global properties as $R = N^{\rm mix}_{+-}/(2\sqrt{N^{\rm mix}_{++}N^{\rm mix}_{--}})$ and is found to deviate significantly from unity only at low $m_{\rm ee}$ ($m_{\rm ee} < 0.2$ GeV/c^2). The raw dielectron yield is then obtained as $S = N^{\rm same}_{+-} - 2R\sqrt{N^{\rm same}_{++}N^{\rm same}_{--}}$. Additional photon conversion rejection is achieved at low $m_{\rm ee}$ ($m_{\rm ee} < 0.1$ GeV/c^2) by removing pairs based on their characteristic orientation relative to the magnetic field quantified by the so-called $\varphi_{\rm V}$ angle defined in Ref. [53]. The remaining contribution of dielectrons from photon conversions is found to be negligible, below 1%. The opposite-sign pair spectrum, the combinatorial background and the extracted raw dielectron yield are shown on the left panel of Fig. 1 as a function of $m_{\rm ee}$ in the 10% most central Pb–Pb collisions, together with the S/B ratio on the right panel.

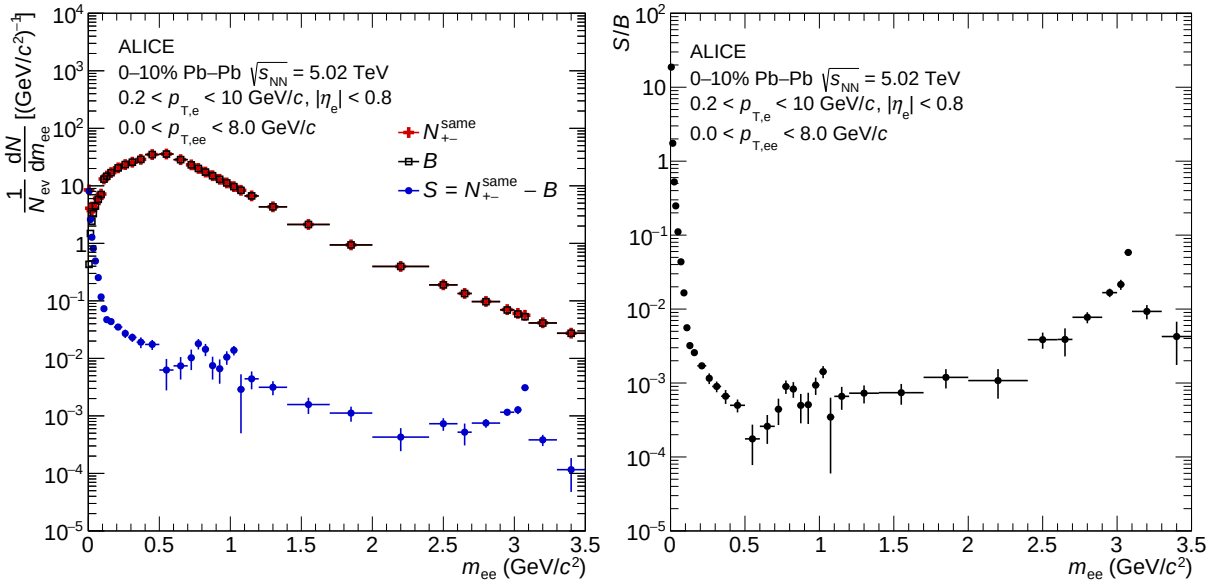

Figure 1: Raw yield (S) overlaid with the opposite-sign pair distribution and the combinatorial background (left panel), as well as signal-over-background ratio (right panel), in the 10% most central Pb–Pb collisions at $\sqrt{s_{\rm NN}} = 5.02$ TeV.

3.2 Yield corrections

The corrected yield of e$^+$e$^-$ pairs in the ALICE acceptance (0.2 or 0.4 $< p_{\rm T,e} <$ 10 GeV/c and $|\eta_{\rm e}| < 0.8$) before integration over one or the other variables is expressed as

$$\frac{{\rm d}^3N_{\rm e^+e^-}}{{\rm d}m_{\rm ee}{\rm d}p_{\rm T,ee}{\rm d}\mathrm{DCA_{ee}}} = \frac{1}{\Delta p_{\rm T,ee}}\frac{1}{\Delta m_{\rm ee}}\frac{1}{\Delta\mathrm{DCA_{ee}}}\frac{S(m_{\rm ee}, p_{\rm T,ee}, \mathrm{DCA_{ee}})}{\varepsilon^{\rm ee}_{\rm rec}(m_{\rm ee}, p_{\rm T,ee}) \times N_{\rm events}}, \tag{2}$$

where $\Delta p_{\rm T,ee}$, $\Delta m_{\rm ee}$ and $\Delta{\rm DCA}_{\rm ee}$ are the width of the $p_{\rm T,ee}$, $m_{\rm ee}$ and ${\rm DCA}_{\rm ee}$ intervals, respectively. The pair efficiency $\varepsilon^{\rm ee}_{\rm rec}(m_{\rm ee}, p_{\rm T,ee})$, including all tracking and PID selection criteria, is calculated using detailed MC simulations. A realistic detector response is modelled using GEANT 3 [71] with the same detector configurations as in data and the DCA detector resolution is corrected a posteriori to reproduce the one measured in the data. To estimate $\varepsilon^{\rm ee}_{\rm rec}(m_{\rm ee}, p_{\rm T,ee})$ with a high statistical precision, samples of dielectron sources are embedded into hadronic collisions simulated with the HIJING event generator [72]. Light-flavor hadrons (π^0,η,η',ρ,ω, and ϕ) and J/ψ mesons, forced to decay into dielectrons with a phenomenological generator [70] and PHOTOS [73], respectively, are used together with an enriched sample of heavy-flavor hadron sources with enforced semileptonic decay channels generated with the Perugia 2011 tune [74] of PYTHIA 6.4 [75]. The pair efficiency is computed as explained in Ref. [68]. Since the reconstruction efficiency for single electron tracks does not show any significant dependence on the electron DCA, for which loose selection criteria are applied, $\varepsilon^{\rm ee}_{\rm rec}(m_{\rm ee}, p_{\rm T,ee})$ is applied to the data as a function of $m_{\rm ee}$ and $p_{\rm T,ee}$. The average reconstruction efficiency of a signal $\rm e^+e^-$ pair ranges from 15% to 25%.

3.3 Systematic uncertainties of measured dielectron spectra

The systematic uncertainties on the measured $p_{\rm T,ee}$- and $m_{\rm ee}$-differential yields originate from tracking, electron identification and purity, and background subtraction. They are evaluated by simultaneous variations of the tracking and PID selection criteria, as described in Ref. [70], implying relative changes of the pair efficiencies and S/B ratio by up to 30% and 40%, respectively. In particular, modifying the requirements on the ITS, TPC and TOF PID signals allows for probing possible biases due to differences in the detector responses in data and MC and remaining hadron contamination in the electron sample. The systematic uncertainty is calculated as the root mean square of the variation of the data points. It is found to be larger at low $p_{\rm T,ee}$, up to about 10% for $p_{\rm T,ee} < 2$ GeV/c where the S/B is smaller. Similar to Ref. [68], additional uncertainties related to the conversion rejection criterion ($\varphi_{\rm V}$), the criteria on the number of shared ITS clusters, and the requirement of a hit in the first ITS layer, as well as to the TPC–ITS and TPC–TOF matching efficiencies, are added in quadrature. The first two sources of systematic uncertainties are estimated by varying the selection criteria, whereas the others are determined for single electrons and propagated to the $\rm e^+e^-$ pairs using a MC method. The resulting systematic uncertainties are listed in Table 1.

An additional source of systematic uncertainty is considered for the ${\rm DCA}_{\rm ee}$-differential analysis. To take into account possible systematic effects related to the correlation between $p_{\rm T,ee}$ and ${\rm DCA}_{\rm ee}$, the latter is studied in each mass region under interest. The difference of the pair efficiency at the maximum and minimum mean $p_{\rm T,ee}$, seen as a function of ${\rm DCA}_{\rm ee}$, in a given mass region is used to assign a systematic uncertainty [70]. It is found to be of the order of 3%. The total systematic uncertainty is given in Table 1 for the $p_{\rm T,ee}$ and $m_{\rm ee}$ analysis, as well as the ${\rm DCA}_{\rm ee}$ analysis.

4 Estimation of hadronic sources

The dielectron measurement is compared with the sum of expected contributions from light- and heavy-flavor hadron decays within the kinematic range under study, i.e. the hadronic cocktail. They are estimated with simulations including the angular, momentum and DCA resolution of the detector for the given data-taking period, as well as bremsstrahlung effects, which are not corrected for in the data analysis [70, 76].

Table 1: Summary of the total systematic uncertainties of the measured dielectron yields in the 10% most central Pb–Pb collisions at $\sqrt{s_{\rm NN}} = 5.02$ TeV. The values presented as a range correspond to the smallest and largest observed systematic uncertainties.

Analysis /sources	$(m_{\rm ee}, p_{\rm T,ee})$	$\rm DCA_{ee}$
Tracking and PID selection	5–11%	4–11%
Conversion rejection	2–4%	N/A
Number of shared ITS clusters	4–12%	4–12%
Hit in the first ITS layer	3%	3%
TPC–ITS matching	8–12%	8–12%
TPC–TOF matching	0–3%	0–3%
$\rm DCA_{ee}$–$p_{\rm T,ee}$ correlation	N/A	3%
Total	12–20%	15–21%

4.1 Dielectron yield from hadronic decays as a function of $m_{\rm ee}$ and $p_{\rm T,ee}$

4.1.1 Decays of light-flavor hadrons and J/ψ mesons

The expected dielectron yield from the decays of known light-flavor (π^0, η, η', ω, ρ, ϕ) and J/ψ hadrons is calculated as described in Ref. [68]. Parameterizations of the $p_{\rm T}$-differential yields of the different hadrons are taken as input to a fast Monte Carlo simulation, that performs the decays and allows retrieving the corresponding expected dielectron yields [70]. Since the $\pi^{\pm}$ measurement extends down to $p_{\rm T} = 0.1$ GeV/c and exhibits small uncertainties [77], charged pions are used to approximate neutral pions. An additional 10% systematic uncertainty is considered to take into account differences due to isospin-violating decays as described in Refs. [68, 78]. The $p_{\rm T}$ spectrum of η is computed using the same approach as in Ref. [79]. First, the η/π^0 ratios measured as a function of $p_{\rm T}$ in hadronic collisions by ALICE [80–83] and CERES/TAPS [84] at different energies are parameterized to obtain a pp reference. Second, radial flow effects in Pb–Pb collisions are evaluated with the double ratio of the $\rm K^{\pm}/\pi^{\pm}$ $p_{\rm T}$ spectra measured at midrapidity ($|y| < 0.5$) in the 10% most central Pb–Pb collisions and in pp collisions [77]. Due to their similar masses, $\rm K^{\pm}$ and η are expected to be affected by radial flow in a similar way. The corresponding η/π^0 ratio in central Pb–Pb collisions is computed as

$$\left(\frac{\eta}{\pi^0}\right)_{\rm PbPb} = \left(\frac{\eta}{\pi^0}\right)_{\rm pp} \times R_{\rm flow} = \left(\frac{\eta}{\pi^0}\right)_{\rm pp} \times \frac{\left(\frac{\rm K^{\pm}}{\pi^{\pm}}\right)^{*}_{\rm PbPb}}{\left(\frac{\rm K^{\pm}}{\pi^{\pm}}\right)^{*}_{\rm pp}}, \tag{3}$$

where * means that the value is not taken at $p_{\rm T}$ but $m_{\eta}/m_{\rm K^{\pm}} \times p_{\rm T}$ to take into account the small difference in mass between η and $\rm K^{\pm}$ of about 10%. In the left panel of Fig. 2, the correction factor $R_{\rm flow}$ is presented for the 0–5% and 5–10% centrality intervals based on the $\rm K^{\pm}$ and $\pi^{\pm}$ measurements [77], considering the systematic uncertainties of the published $\rm K^{\pm}/\pi^{\pm}$ ratios as uncorrelated between the Pb–Pb and pp colliding systems. For $p_{\rm T} < 9$ GeV/c $R_{\rm flow}$ is consistent with unity and an universal constant behavior in hadronic and heavy-ion collisions is assumed. The resulting η/π^0 ratio in central Pb–Pb collisions is parameterized as a function of $p_{\rm T}$ for the two centrality classes separately, as shown in the right panel of Fig. 2 together with the measured η/π^0 ratios in hadronic collisions [80–84]. A similar trend is observed in central Pb–Pb collisions at $\sqrt{s_{\rm NN}} = 2.76$ TeV, where the η/π^0 ratio was measured by the ALICE collaboration [85] at midrapidity. The corresponding calculated dielectron yields in both centrality classes are combined together to obtain the expected $\rm e^+e^-$ yield in the 10% most central Pb–Pb collisions assuming fully correlated systematic uncertainties of the η/π^0 ratios. The η', ω, and ρ $p_{\rm T}$ distributions are generated assuming $m_{\rm T}$-scaling, implying that the spectra of all light mesons as a function of $m_{\rm T} = \sqrt{m^2 + p_{\rm T}^2}$ follow a universal form and differ only by a normalization factor. Finally,

the measured ϕ [86] and J/ψ [87] $p_{\rm T}$-differential yields in central Pb–Pb collisions are fitted and in case of the ϕ extrapolated down to low $p_{\rm T}$ ($p_{\rm T} < 0.4$ GeV/c) using $m_{\rm T}$-scaling.

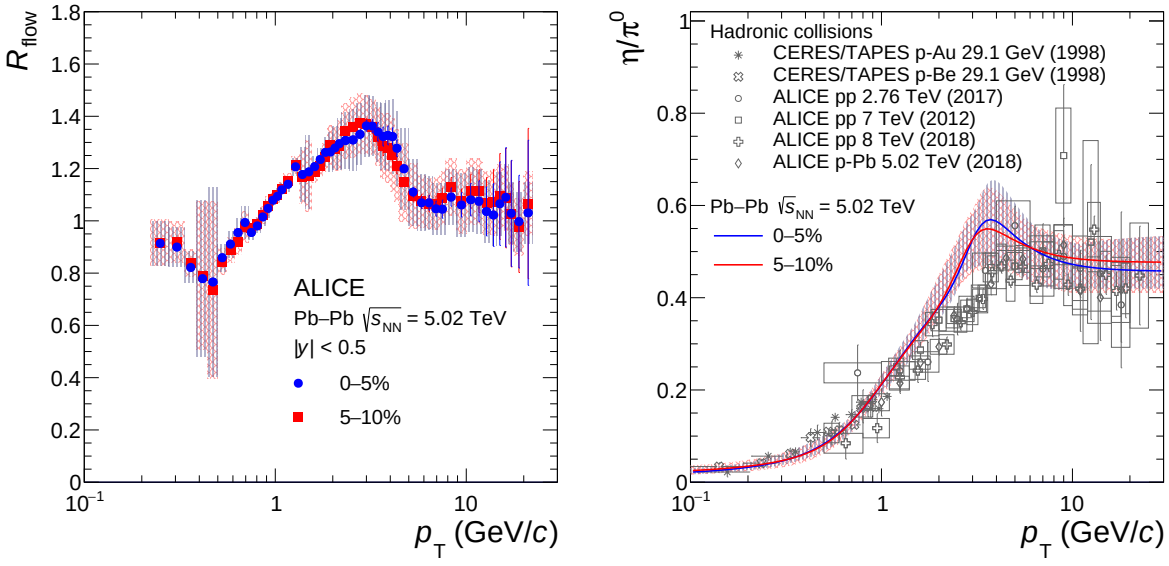

Figure 2: Left panel: double ratio of the measured $\mathrm{K}^{\pm}/\pi^{\pm}$ $p_{\rm T}$ spectra in central Pb–Pb collisions and in pp collisions at $\sqrt{s_{\rm NN}} = 5.02$ TeV [77] dilated as a function of $p_{\rm T}$ by the ratio of the η and $\mathrm{K}^{\pm}$ meson mass (see text). Right panel: measured [80–84] and parameterized $\frac{\eta}{\pi^0}$ ratios in hadronic collisions and central Pb–Pb collisions, respectively.

4.1.2 Open-charm and open-beauty hadron decays

Two different calculations for the contributions of correlated semileptonic heavy-flavor hadron decays are considered. One is based on the dielectron measurements in pp collisions at the same center-of-mass energy per nucleon pair [90] scaled with the average number of binary nucleon–nucleon collisions $\langle N_{\rm coll} \rangle$. The resulting cocktail is called in the following $N_{\rm coll}$-scaled HF cocktail. For this purpose, the expected $\mathrm{e}^+\mathrm{e}^-$ yields of correlated semileptonic heavy-flavor hadron decays, estimated with the POWHEG event generator [91–94] using PYTHIA 6 [75] as parton shower, are first fitted to the measured $\mathrm{e}^+\mathrm{e}^-$ spectra in pp collisions to extract $\mathrm{d}\sigma_{\mathrm{c\bar{c}}}/\mathrm{d}y|_{y=0}$ and $\mathrm{d}\sigma_{\mathrm{b\bar{b}}}/\mathrm{d}y|_{y=0}$, as explained in Ref. [90]. The calculations are then scaled with the average nuclear overlap function in the 0–10% centrality interval. The uncertainties originating from the branching ratio of the semileptonic decays of the open heavy-flavor hadrons and the fragmentation functions of charm and beauty quarks are omitted assuming that these do not change from pp to central Pb–Pb collisions. This approach ignores shadowing and suppression effects due to the interactions of charm and beauty quarks with other partons in the medium, as well as any modification of the hadronization processes. Measurements of the nuclear modification factor $R_{\rm AA}^{\rm c,b\to e^{\pm}}$ of single electrons from charm and beauty hadron decays, however, do show significant modifications of the $p_{\rm T}$ spectra in Pb–Pb collisions compared to pp collisions [88]. These modifications are due to initial cold nuclear matter (CNM) effects as well as final hot nuclear matter (HNM) effects like partonic energy loss and collective flow. Both affect differently the $\mathrm{e}^+\mathrm{e}^-$ pairs. Whereas the former alters the initial production of heavy-quark pairs and per consequence of dielectrons, the latter acts on the e^+ and e^- mostly independently with the exception of flow.

In a second approach, a simple model is considered to include the single heavy-flavor decay electron measurements in the cocktail inputs. First, CNM and HNM effects are disentangled assuming

$$R_{\rm AA}^{\rm c,b\to e^{\pm}} = R_{\rm AA,CNM}^{\rm c,b\to e^{\pm}} \times R_{\rm AA,HNM}^{\rm c,b\to e^{\pm}}, \tag{4}$$

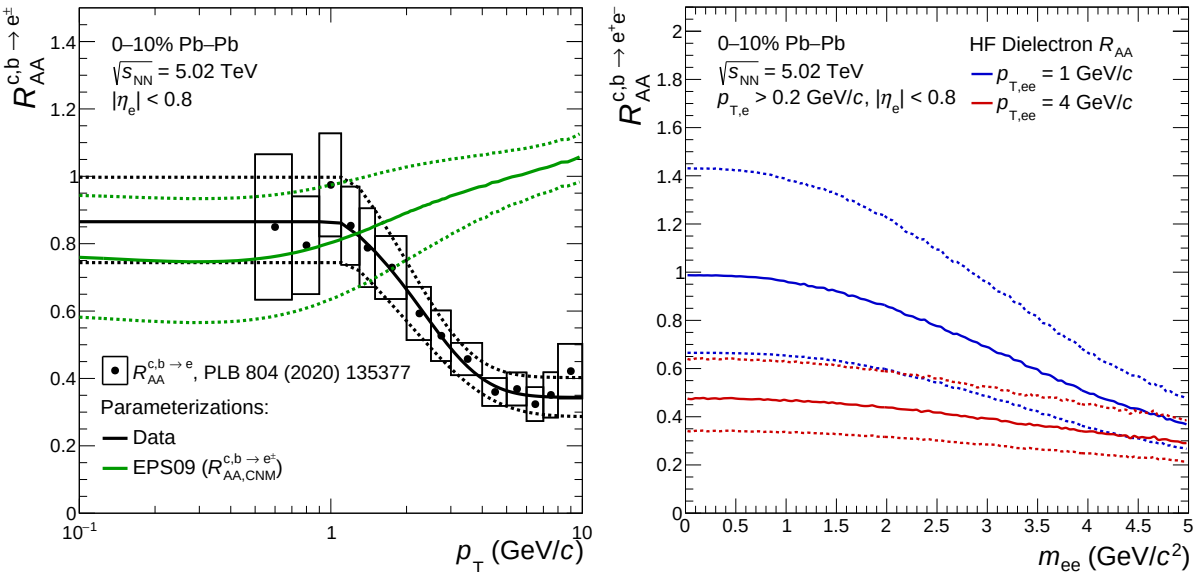

Figure 3: Left panel: measured nuclear modification factor of single electrons from heavy-flavor hadron decays [88], as well as its parameterization and the estimated nuclear modification factor caused by pure cold-nuclear matter effects with EPS09 nPDFs [89], in the 10% most central Pb–Pb collisions at $\sqrt{s_{\rm NN}} = 5.02$ TeV. Right panel: resulting nuclear modification factor of $\rm e^+e^-$ pairs from correlated open heavy-flavor hadron decays computed with a toy MC (see text) for two different $p_{\rm T,ee}$.

where $R_{\rm AA}^{\rm c,b\to e^{\pm}}$ is the parameterized single-electron measurement and $R_{\rm AA,CNM}^{\rm c,b\to e^{\pm}}$ is computed using the EPS09 nuclear parton distribution function (nPDF) [89]. Both are shown as a function of $p_{\rm T}$ on the left panel of Fig. 3, together with the measured nuclear modification factor of heavy-flavor decay electrons in the 10% most central Pb–Pb collisions at $\sqrt{s_{\rm NN}} = 5.02$ TeV. The modifications are then propagated to $\rm e^+e^-$ pairs using Monte Carlo simulations and a weighting procedure. The HNM effects are assumed to fully factorize between the $\rm e^+$ and $\rm e^-$:

$$R_{\rm AA,HNM}^{\rm c,b\to e^+e^-} = R_{\rm AA,HNM}^{\rm c,b\to e^{\pm}}(p_{\rm T,e^+}) \times R_{\rm AA,HNM}^{\rm c,b\to e^{\pm}}(p_{\rm T,e^-}), \tag{5}$$

where $R_{\rm AA,HNM}^{\rm c,b\to e^+e^-}$ is the dielectron nuclear modification factor due to HNM effects. Similarly, the CNM effects are estimated on the $\rm e^+e^-$ pair with the dielectron nuclear modification factor due to CNM effects ($R_{\rm AA,CNM}^{\rm c,b\to e^+e^-}$) by taking the mean of the single electron $R_{\rm AA,CNM}^{\rm c,b\to e^{\pm}}$

$$R_{\rm AA,CNM}^{\rm c,b\to e^+e^-} = \frac{R_{\rm AA,CNM}^{\rm c,b\to e^{\pm}}(p_{\rm T,e^+}) + R_{\rm AA,CNM}^{\rm c,b\to e^{\pm}}(p_{\rm T,e^-})}{2}. \tag{6}$$

The resulting dielectron nuclear modification factor ($R_{\rm AA}^{\rm c,b\to e^+e^-}$),

$$R_{\rm AA}^{\rm c,b\to e^+e^-} = R_{\rm AA,CNM}^{\rm c,b\to e^+e^-} \times R_{\rm AA,HNM}^{\rm c,b\to e^+e^-}, \tag{7}$$

is reported on the right panel of Fig. 3 for two different $p_{\rm T,ee}$ values as a function of $m_{\rm ee}$. Dielectrons with a large $m_{\rm ee}$ and/or $p_{\rm T,ee}$ originate on average from heavy-flavor hadrons with higher $p_{\rm T}$ than $\rm e^+e^-$ pairs at smaller $m_{\rm ee}$ or $p_{\rm T,ee}$ and are therefore more affected by HNM effects. In this approach, CNM and HNM effects seem to cancel out within large uncertainties at low $m_{\rm ee}$ and $p_{\rm T,ee}$ ($R_{\rm AA,CNM}^{\rm c,b\to e^+e^-} \times R_{\rm AA,HNM}^{\rm c,b\to e^+e^-} \approx 1$). The dielectron $R_{\rm AA}^{\rm c,b\to e^+e^-}$ is then applied to the contributions of correlated semileptonic open-charm and open-beauty hadron decays estimated from pp collisions at the same $\sqrt{s_{\rm NN}}$, as explained above. The resulting cocktail is called $R_{\rm AA}^{\rm c,b\to e^{\pm}}$-modified HF cocktail.

4.1.3 Systematic uncertainties

The systematic uncertainties of the hadronic cocktail originate from the following sources: the $\pi^{\pm}$, ϕ, and J/ψ parameterizations as a function of $p_{\rm T}$, the η/π^0 ratio, the $m_{\rm T}$-scaling parameters used for ρ, ω, η' and ϕ, the branching ratios of the different light-flavor hadron decay channels, and the heavy-flavor cross sections in pp collisions. In case of the $N_{\rm coll}$-scaled HF cocktail, the nuclear overlap function is also considered as a source of uncertainty, whereas for the $R_{\rm AA}^{\rm c,b\rightarrow e^{\pm}}$-modified HF cocktail the uncertainties of the measured $R_{\rm AA}^{\rm c,b\rightarrow e^{\pm}}$ and the EPS09 nPDF are propagated to the final expected dielectron yield resulting in two uncorrelated uncertainties of similar magnitude depending on $m_{\rm ee}$ and $p_{\rm T,ee}$. The different contributions added in quadrature amount to a total systematic uncertainty between 10% and 20% depending on $m_{\rm ee}$ and $p_{\rm T,ee}$ for the $N_{\rm coll}$-scaled HF cocktail. The $R_{\rm AA}^{\rm c,b\rightarrow e^{\pm}}$-modified HF cocktail has significantly larger uncertainties, where the heavy-flavor contributions are dominant, i.e. up to about 40% in the intermediate-mass range ($1.2 < m_{\rm ee} < 2.6$ GeV/c^2).

4.2 $\rm DCA_{ee}$ template distributions

The $\rm DCA_{ee}$ distributions of the different dielectron sources are determined by the convolution of the DCA detector resolution, the decay length of the mother particles, and the decay kinematics. Dielectrons produced at the primary vertex are expected to have smaller $\rm DCA_{ee}$ than $\rm e^+e^-$ pairs originating from the decays of correlated open-charm and open-beauty hadrons with finite decay lengths ($c\tau_{\rm D} \approx 150$ μm and $c\tau_{\rm B} \approx 470$ μm). A full GEANT 3 [71] simulation of the ALICE central barrel, tuned to describe the performance of each detector subsystem, in particular the ITS, is utilized. The same analysis selection criteria as in data are applied to extract the $\rm DCA_{ee}$ spectra of $\rm e^+e^-$ pairs originating from the decays of prompt and non-prompt J/ψ mesons, as well as open-beauty and open-charm hadrons. Contrary to open-beauty hadrons, the various open-charm hadrons have significantly different decay lengths (e.g. 59.9 μm for $\Lambda_{\rm c}^{\pm}$ and 311.8 μm for $\rm D^{\pm}$ mesons [95]). Therefore their relative yields are particularly relevant. The measured production ratios of prompt open-charm hadrons in pp [96, 97] and Pb–Pb collisions [98], together with their semileptonic decay branching ratios [95], are used to obtain the $\rm c\bar{c}$ $\rm DCA_{ee}$ distribution calculated as the combination of semi-leptonic decays of the different open-charm hadrons. The $\rm D^{\pm}/D^0$ ratio is found to be similar in pp and Pb–Pb collisions, whereas possible enhancements of the $\rm D_s^{\pm}/D^0$ and $\Lambda_{\rm c}/\rm D^0$ ratios in Pb–Pb compared to pp collisions are taken into account. Finally, the fraction of non-prompt J/ψ, $f_{\rm B}$, as a function of $p_{\rm T}$ measured by ALICE [87] in central Pb–Pb collisions is taken as input to build the inclusive $\rm DCA_{ee}$ template of the J/ψ. Each contribution is normalized to its expected yield from the hadronic cocktail in the same $m_{\rm ee}$ and $p_{\rm T,ee}$ range after the same fiducial selection criteria ($|\eta_{\rm e}| < 0.8$ and $p_{\rm T,e} > 0.4$ GeV/c).

Three sources of systematic uncertainties additional to those mentioned in Section 4.1.3, depending on $\rm DCA_{ee}$, are considered and added in quadrature. First, the DCA single-track resolution is not perfectly reproduced in the simulation. The DCA templates obtained with MC simulations using a post-correction of the DCA resolution in order to reproduce the one in data are compared to those estimated without. As a conservative estimate, half of the difference between the two spectra is attributed to the systematic uncertainty. This leads to a systematic uncertainty between 10 and 25% varying with the $\rm DCA_{ee}$ value for prompt $\rm e^+e^-$ pairs, while for non-prompt dielectrons ($\rm c\bar{c}$ and $\rm b\bar{b}$) a maximum of 10% systematic uncertainty is observed at small $\rm DCA_{ee}$, i.e. for $\rm DCA_{ee}$ values smaller than one. Second, the uncertainties of the charm and beauty-hadron production ratios, of their semileptonic decay branching ratios, and of $f_{\rm B}$ are propagated to the corresponding $\rm DCA_{ee}$ distributions and amount to about 10%. Third, the uncertainty related to the $p_{\rm T}$ spectra of the open-charm and open-beauty mother hadrons is found to be of the order of 5% at large $\rm DCA_{ee}$.

5 Inclusive dielectron production

5.1 Dielectron invariant-mass spectra

The yield of e^+e^- pairs in the ALICE acceptance ($|\eta_e| < 0.8$ and $0.2 < p_{T,e} < 10$ GeV/c) is shown as a function of m_{ee} in the 10% most central Pb–Pb collisions at $\sqrt{s_{\rm NN}} = 5.02$ TeV in Fig. 4. In the left panel, the data are compared with the expected contributions from known hadronic sources, i.e. the $R_{\rm AA}^{\rm c,b\to e^{\pm}}$-modified HF cocktail shown with dashed lines and the $N_{\rm coll}$-scaled HF cocktail displayed as full lines, both explained in Section 4.1.2. In the π^0 ($m_{ee} < 0.135$ GeV/c^2) and J/ψ ($2.7 < m_{ee} < 3.3$ GeV/c^2) mass regions, where dielectrons from π^0-Dalitz and J/ψ decays are expected to dominate the yield of e^+e^- pairs, respectively, the data are well reproduced by the hadronic cocktails.

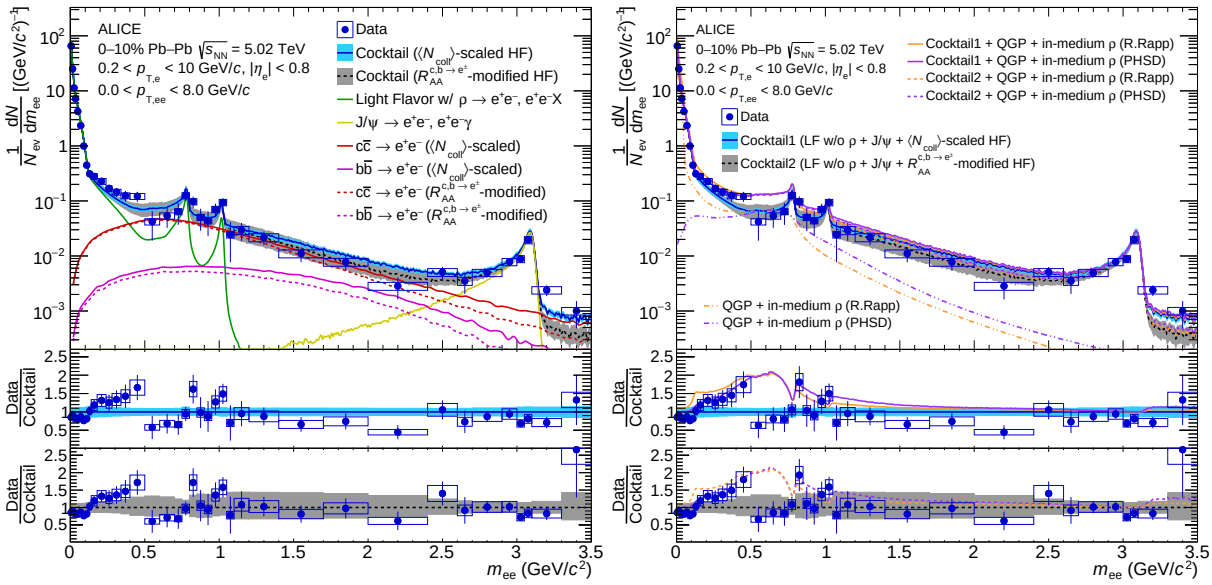

Figure 4: Upper panels: dielectron m_{ee}-differential yields in the 10% most central Pb–Pb collisions at $\sqrt{s_{\rm NN}} = 5.02$ TeV, compared with the expected e^+e^- contributions from known hadronic decays, including two different estimations for dielectrons from correlated heavy-flavor hadron decays (left panel), and two predictions for thermal radiation from the medium [36, 99] (right panel). Bottom panels: ratios data to cocktails, together with the expected ratios from the models. The error bars and boxes represent the statistical and systematic uncertainties of the data, respectively, whereas the bands show the uncertainties of the hadronic cocktails.

In the bottom and middle left panels of Fig. 4, the ratio of the data and the different hadronic cocktails are presented. At low m_{ee} ($0.18 < m_{ee} < 0.5$ GeV/c^2), the ratios are systematically above one, although consistent with unity within 1.7σ (1.5σ) for the $N_{\rm coll}$-scaled ($R_{\rm AA}^{\rm c,b\to e^{\pm}}$-modified) HF cocktail. The hint for an excess does not depend significantly on the method used to estimate the heavy-flavor contribution. In both cocktails, the contribution from ρ mesons is estimated neglecting any medium effect and amounts to about 18% of the total yield of known hadronic sources at m_ρ. However, a significant contribution of e^+e^- pairs originating from ρ mesons produced thermally in the medium is expected at low m_{ee}. Due to its short lifetime compared to the one of the hot fireball and its strong coupling to the $\pi^+\pi^-$ channel, the ρ meson is likely to be regenerated in the hot hadronic phase with a medium-modified spectral function broader than in vacuum. In the intermediate-mass range (IMR), i.e. $1.2 < m_{ee} < 2.6$ GeV/c^2, the heavy-flavor modified cocktail can better describe the data, systematically below the expectations from the $N_{\rm coll}$-scaled HF cocktail. Nevertheless, the former cocktail suffers from large uncertainties.

In the right panel of Fig. 4, the data are compared with the $R_{\rm AA}^{\rm c,b\to e^{\pm}}$-modified and the $N_{\rm coll}$-scaled HF cocktails excluding the contribution from the ρ meson. In addition, expectations from two theoretical models

for thermal dielectrons from the partonic and hadronic phase, referred to as QGP and in-medium ρ, are shown. As for the hadronic cocktail, detector resolution effects were applied to the predictions [68, 76]. In both calculations, ρ mesons produced in the hot hadronic phase are a relevant source of thermal radiation for $m_{\rm ee} < 0.8$ GeV/c^2. The model from R. Rapp [36] is an expanding fireball model, where the thermal emission rate of dielectrons from the hadronic phase is calculated based on a hadronic many-body theory with in-medium modified ρ, whereas a lattice-QCD inspired approach is used for the equation of state in the QGP. The Parton-Hadron-String Dynamics (PHSD) model is a transport model [99] with in-medium modified electromagnetic spectral functions of low-mass vector mesons. The predictions were added to the hadronic cocktails to obtain the total expected yield of dielectrons. In the bottom and middle right panels of Fig. 4, the ratio between the data and the different hadronic cocktails excluding the ρ meson contribution are shown together with the ratio of the total expected dielectron yield to the hadronic cocktails. The data-to-cocktail ratio integrated in the $m_{\rm ee}$ range $0.18 < m_{\rm ee} < 0.5$ GeV/c^2 is found to be $R = 1.42 \pm 0.12$ (stat.) ± 0.17 (syst.) ± 0.12 (cocktail) for the $N_{\rm coll}$-scaled HF cocktail and $R = 1.44 \pm 0.12$ (stat.) ± 0.17 (syst.)$^{+0.17}_{-0.21}$ (cocktail) for the $R_{\rm AA}^{\rm c,b\to e^{\pm}}$-modified HF cocktail, where the systematic uncertainty related to the cocktail is reported separately to those originating from the data. Both are consistent with the predicted ratios using the model calculations for thermal contributions and the hadronic cocktails. Both models can reproduce the data for $0 < m_{\rm ee} < 0.5$ GeV/c^2, but tend to overestimate them for $0.5 < m_{\rm ee} < 0.7$ GeV/c^2. In the IMR, the QGP is the main source of predicted thermal radiation. The expected thermal contribution to the total dielectron yield is small, i.e. around 15% integrated over this mass range, which is below the sensitivity of the data and much smaller than the uncertainties of the heavy-flavor modified cocktail.

To better investigate the hint for an excess of $\rm e^+e^-$ pairs at low $m_{\rm ee}$, the expected dielectron yield from known hadronic sources is subtracted from the data to obtain a so-called excess spectrum. The excess spectra computed with the two different cocktails ($R_{\rm AA}^{\rm c,b\to e^{\pm}}$-modified and $N_{\rm coll}$-scaled HF cocktails) are shown in Fig. 5 for $0.14 < m_{\rm ee} < 1.1$ GeV/c^2. Upper limits at 90% C.L. using the Feldman and Cousins method [100] are reported for the values which are found to be statistically consistent with zero within one standard deviation. In the $m_{\rm ee}$ range $0.18 < m_{\rm ee} < 0.5$ GeV/c^2, where the significance of the excess reaches 1.53σ and 1.79σ using the $R_{\rm AA}^{\rm c,b\to e^{\pm}}$-modified and $N_{\rm coll}$-scaled HF cocktails, respectively, the result is not very sensitive to the different implementations of the heavy-flavor background. The excess spectra are compared with the same models [36, 99] as above. The computed contributions from ρ mesons produced thermally in the hot hadronic matter and thermal radiation from the QGP are shown separately. In the case of the PHSD model (right panel of Fig. 5), the dielectron production in the QGP is calculated by implementing the off-shell cross sections of $\rm q\overline{q} \to e^+e^-$, $\rm q\overline{q} \to e^+e^-g$ and $\rm qg \to qe^+e^-$ ($\rm \overline{q}g \to \overline{q}e^+e^-$) reactions from the dynamical quasiparticle model [101] into the PHSD transport approach. The yield of thermal radiation from the hadronic phase (in-medium ρ) predicted by PHSD is smaller than the one estimated by the model of R. Rapp (right panel of Fig. 5) [36]. Both calculations are nevertheless compatible with the data within their statistical and systematic uncertainties.

5.2 Dielectron $p_{\rm T,ee}$ spectra

The yield of $\rm e^+e^-$ pairs in the $m_{\rm ee}$ range where a hint for an excess is observed and the heavy-flavor contribution is expected to be still relatively small ($0.18 < m_{\rm ee} < 0.34$ GeV/c^2) is shown as a function of $p_{\rm T,ee}$ in the left panel of Fig. 6. The data are compared with the two different cocktails discussed in Sec. 4. In this $m_{\rm ee}$ range, η Dalitz decays ($\eta \to \gamma \rm e^+e^-$) are expected to contribute significantly at low $p_{\rm T,ee}$, whereas correlated open-beauty hadron decays play a role at high $p_{\rm T,ee}$. The data-to-cocktail ratios, shown on the bottom and middle left panels of Fig. 6, are consistent with unity, while being systematically above but still within 1.53σ (1.45σ) in the $p_{\rm T,ee}$ range $0.9 < p_{\rm T,ee} < 2$ GeV/c for the $N_{\rm coll}$-($R_{\rm AA}^{\rm c,b\to e^{\pm}}$)-modified HF cocktail. The ratios are compared with the expected inclusive dielectron yield-to-cocktail ratio estimated with the two different calculations for thermal radiation from the partonic and hadronic phase [36, 99] presented in Sec. 5.1. Both models predict thermal contributions relevant only

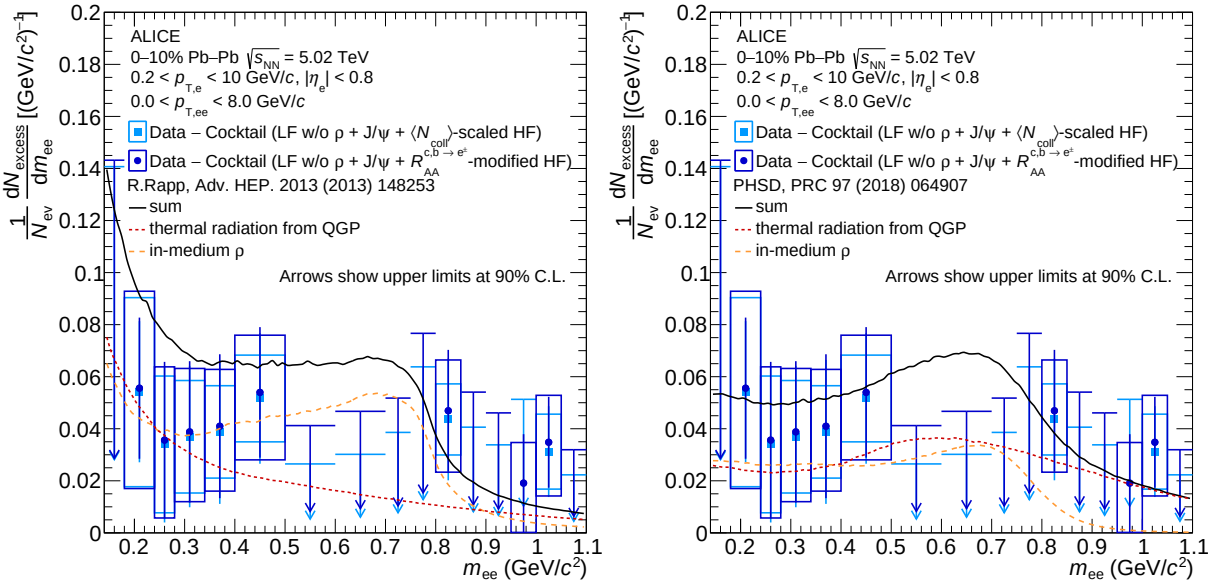

Figure 5: Excess yield of dielectrons in the 10% most central Pb–Pb collisions at $\sqrt{s_{\rm NN}} = 5.02$ TeV with respect to the expected $\rm e^+e^-$ contributions from known hadronic sources, including or not including medium effects for the heavy-flavor contributions, and compared with predictions from the model of R. Rapp [36] (left) and from the PHSD transport approach [99] (right).

at low $p_{\rm T,ee}$ ($p_{\rm T,ee} < 4$ GeV/c) and are compatible with the data within uncertainties.

The IMR is dominated by correlated $\rm e^+e^-$ pairs from semileptonic decays of charm and beauty hadrons. The $p_{\rm T,ee}$-differential yield of $\rm e^+e^-$ pairs measured in this $m_{\rm ee}$ region is shown in comparison with the two different hadronic cocktails, as well as predictions for thermal radiation [36, 99] in the data-to-cocktail ratios, in the right panel of Fig. 6. The contribution of $\rm e^+e^-$ pairs from $\rm c\bar{c}$ is expected to be the dominant dielectron source for $p_{\rm T,ee} < 2$ GeV/c, whereas most of the $\rm e^+e^-$ pairs originate from $\rm b\bar{b}$ for $p_{\rm T,ee} > 4$ GeV/c. The data are systematically below the $N_{\rm coll}$-scaled HF cocktail, particularly at high $p_{\rm T,ee}$ where the difference reaches 2σ in the last $p_{\rm T,ee}$ interval ($6 < p_{\rm T,ee} < 8$ GeV/c). This is in agreement with a heavy-flavor suppression, increasing with $p_{\rm T,ee}$, with respect to pp collisions at the same center-of-mass energy per nucleon pair. The trend is reproduced by the $R_{\rm AA}^{\rm c,b\to e^{\pm}}$-modified HF cocktail based on the measured single heavy-flavor decay electron $R_{\rm AA}$ [88], although this cocktail has large uncertainties. The contribution of thermal radiation from the QGP is predicted to be at most 15% of the inclusive dielectrons for $p_{\rm T,ee} < 2$ GeV/c, as can be seen on the bottom and middle right panels of Fig. 6. It is much smaller than the uncertainties of the heavy-flavor modified cocktail. Therefore a different approach is mandatory to address the production of $\rm e^+e^-$ pairs in the partonic phase.

6 Topological separation of $\rm e^+e^-$ sources

Dielectron measurements in the IMR provide a handle to disentangle the contributions of hadronic and QGP thermal radiation. However, dielectrons from correlated heavy-flavor hadron decays dominate the $\rm e^+e^-$ pair production in this phase space and make the extraction of the thermal QGP signal very challenging. The pair $\rm DCA_{ee}$ variable offers experimental means to disentangle displaced dielectrons produced in the decays of heavy-flavor hadrons from a prompt thermal contribution.

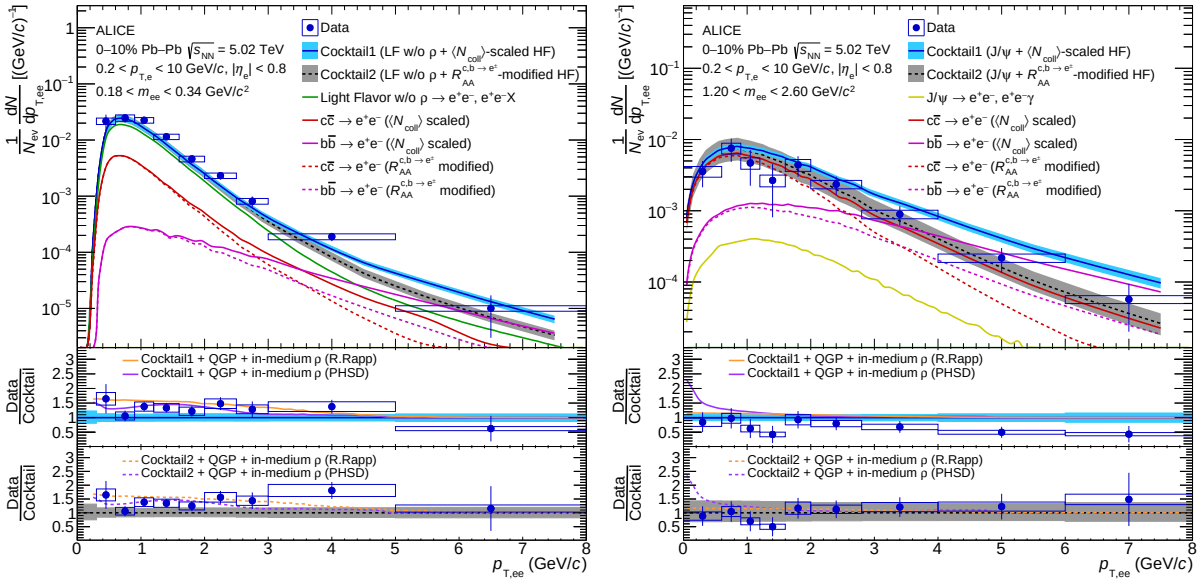

Figure 6: Upper panels: dielectron $p_{\rm T,ee}$-differential yields in two different $m_{\rm ee}$ ranges, $0.18 < m_{\rm ee} < 0.34$ GeV/c^2 (left) and $1.2 < m_{\rm ee} < 2.6$ GeV/c^2 (right), in the 10% most central Pb–Pb collisions at $\sqrt{s_{\rm NN}} = 5.02$ TeV, compared with the expected $\rm e^+e^-$ contributions from known hadronic decays, including two different estimations for dielectrons from correlated heavy-flavor hadron decays (see text). Bottom panels: ratios data to cocktails, excluding the contribution from vacuum ρ, together with two predictions for thermal radiation from the medium [36, 99]. The error bars and boxes represent the statistical and systematic uncertainties of the data, respectively, whereas the bands show the uncertainties of the hadronic cocktails.

6.1 J/ψ invariant-mass region

The contributions from prompt and non-prompt J/ψ are well constrained by independent ALICE measurements which combine the inclusive yield with the fraction of J/ψ originating from beauty hadron decays [87]. These components are dominant for $2.6 < m_{\rm ee} < 3.1$ GeV/c^2, making this mass range well suited to test the understanding of the detector $\rm DCA_{ee}$ resolution. The measured $\rm DCA_{ee}$-differential yield in this mass range is compared with the different expected hadronic components, i.e. dielectrons from prompt and non-prompt J/ψ decays, as well as from open heavy-flavor hadron decays in Fig. 7. The $R_{\rm AA}^{\rm c,b\to e^\pm}$-modified heavy-flavor calculations are used to estimate the heavy-flavor yields, which are found to be a subleading contribution at all $\rm DCA_{ee}$. The data are described by the sum of the $\rm DCA_{ee}$ templates, validating the description of the $\rm DCA_{ee}$ resolution in the simulations.

6.2 Intermediate-mass range and QGP thermal radiation

The $\rm DCA_{ee}$-differential yield measured in the mass range $1.2 < m_{\rm ee} < 2.6$ GeV/c^2 is shown in Fig. 8 together with the expected contributions of known hadronic decays, including or not including medium effects for dielectrons from heavy-flavor hadron decays ($N_{\rm coll}$-scaled and $R_{\rm AA}^{\rm c,b\to e^\pm}$-modified HF cocktails, respectively). The J/ψ contribution in this mass range originates principally from electrons affected by bremsstrahlung in the detector material and reconstructed with a smaller $p_{\rm T}$ compared to their true one, shifting the measured dielectron invariant mass towards smaller values. The upper boundary of the $m_{\rm ee}$ range (2.6 GeV/c^2) was chosen such that the J/ψ contribution is one order of magnitude smaller than the measured dielectron yield. On the contrary, the $\rm b\bar{b} \to ee$ contribution, with the large decay length of open-beauty hadrons ($c\tau_{\rm B} \approx 470\,\mu$m), dominates the spectrum at high $\rm DCA_{ee}$, while the $\rm c\bar{c} \to ee$ component defines the spectrum at low $\rm DCA_{ee}$ values ($c\tau_{\rm D} \approx 150\,\mu$m). Overall, the data are below the $N_{\rm coll}$-scaled HF cocktail, indicating a heavy-flavor suppression in Pb–Pb collisions compared to pp

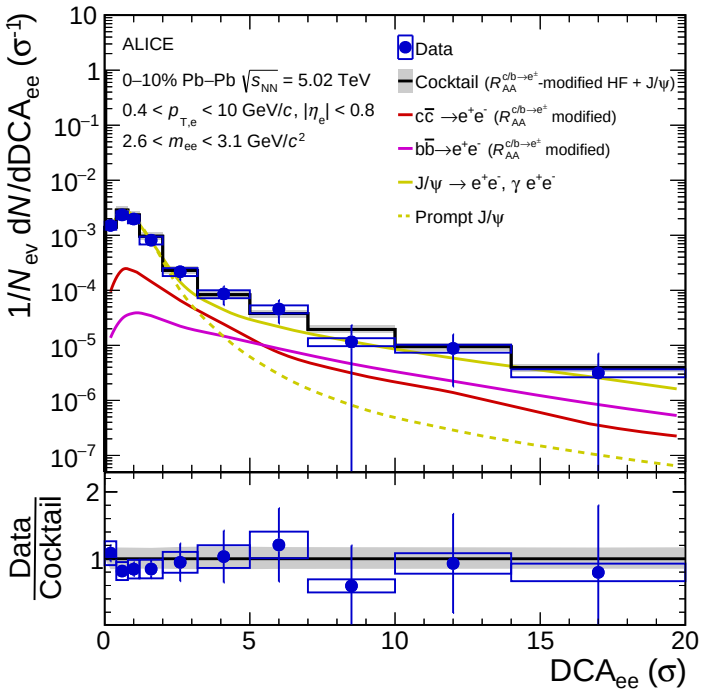

Figure 7: Upper panel: inclusive e^+e^- yield in the 10% most central Pb–Pb collisions at $\sqrt{s_{\rm NN}} = 5.02$ TeV as a function of $\rm DCA_{ee}$ in the mass range $2.6 < m_{\rm ee} < 3.1$ GeV/c^2, compared with a cocktail of expected sources, including medium effects for the heavy-flavor contributions. Bottom panel: corresponding data to cocktail ratio. Statistical and systematic uncertainties on the data are shown as vertical bars and boxes, respectively. The total uncertainty of the cocktail is represented as a grey band.

collisions. A better agreement is observed with the $R_{\rm AA}^{\rm c,b\to e^\pm}$-modified HF cocktail. The data-to-cocktail ratios are compared with the ratio of the total expected dielectron yield and the hadronic cocktail, using predictions for thermal radiation from the two different models [36, 99] discussed in Sec. 5.1. For this purpose, the $\rm DCA_{ee}$ template for prompt e^+e^- pairs is normalized to the expected thermal radiation yield from the models. The contribution of thermal radiation is expected to be between 10 and 40% around $\rm DCA_{ee}$ values of 1.5σ according to these calculations and the $\rm DCA_{ee}$ detector resolution. It is consistent with the data using the $R_{\rm AA}^{\rm c,b\to e^\pm}$-modified HF cocktail to describe the heavy-flavor background.

The description of the data can be improved by fitting the $\rm DCA_{ee}$ templates of the different expected contributions to the data as shown in Fig. 9 (left) and explained below. The J/ψ $\rm DCA_{ee}$ template $\left(f_{\rm DCA}^{\rm fixed}(J/\psi \to e^+e^-)\right)$ is given by the cocktail. The beauty contribution $\left(f_{\rm DCA}^{\rm fixed}(b\bar{b} \to e^+e^-)\right)$ is fixed to reproduce the data at high $p_{\rm T,ee}$ ($p_{\rm T,ee} > 3$ GeV/c). In this $p_{\rm T,ee}$ region, the beauty contribution dominates the spectra, while other components (charm, J/ψ, and thermal) are expected to contribute less than 26% to the dielectron yield. This approach leads to a suppression by a factor 0.74 ± 0.24 (stat.) ± 0.12 (syst.) for beauty compared to $N_{\rm coll}$-scaling. Finally, the data points are fitted with a four-component function

$$f_{\rm DCA} = a \times f_{\rm DCA}({\rm prompt}) + b \times f_{\rm DCA}(c\bar{c} \to e^+e^-) + f_{\rm DCA}^{\rm fixed}(b\bar{b} \to e^+e^-) + f_{\rm DCA}^{\rm fixed}(J/\psi \to e^+e^-), \quad (8)$$

where a and b are the two fit parameters, whereas $f_{\rm DCA}({\rm prompt})$ and $f_{\rm DCA}(c\bar{c} \to e^+e^-)$ are the thermal and open charm contributions, whose yields are given by the model of R. Rapp [36] and the $N_{\rm coll}$-scaled HF cocktail, respectively. The data are found to be consistent with a charm suppression by a factor 0.43 ± 0.4 (stat.) ± 0.22 (syst.) with respect to $N_{\rm coll}$-scaling and an additional prompt component that is a factor 3.17 ± 3.81 (stat.) ± 0.35 (syst.) larger than the predictions from R. Rapp [36] and 1.15 ± 1.38 (stat.) ± 0.13 (syst.) times the expected yield from the PHSD model [99]. The χ^2 of the $\rm DCA_{ee}$ fit is reported as

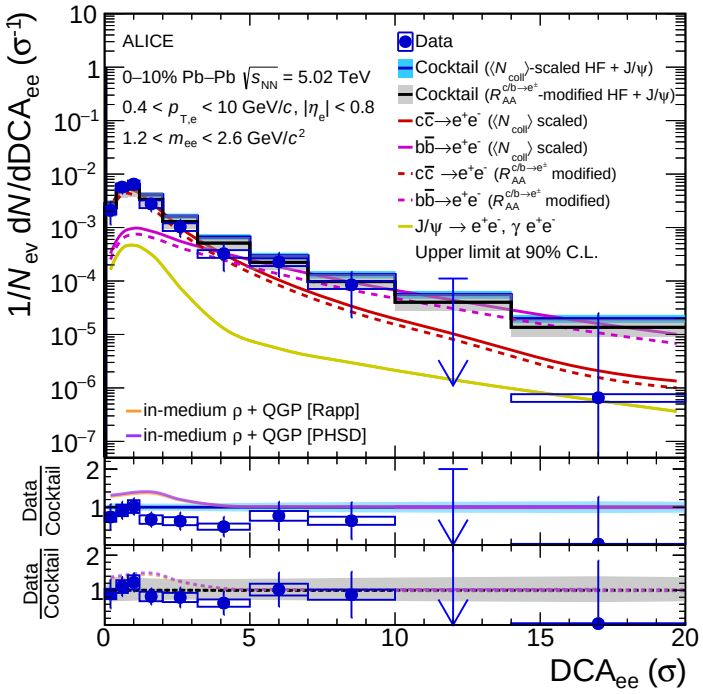

Figure 8: Upper panel: inclusive e^+e^- yield in the 10% most central Pb–Pb collisions at $\sqrt{s_{\rm NN}} = 5.02$ TeV as a function of $\rm DCA_{ee}$ in the mass range $1.2 < m_{\rm ee} < 2.6$ GeV$/c^2$, compared with the expected e^+e^- contributions from known hadronic decays, including two different estimations for dielectrons from correlated heavy-flavor hadron decays (see text). Bottom panels: ratios data to cocktail, together with two predictions for thermal radiation from the medium [36, 99]. Statistical and systematic uncertainties on the data are shown as vertical bars and boxes, respectively. The total uncertainty of the cocktails are represented as band.

a function of the ratio of the yield of e^+e^- pairs originating from a prompt source and from correlated open-charm hadron decays to the total measured dielectron yield on the right-hand panel of Fig. 9. The full line shows the systematic uncertainties originating from those of the data, determined by moving the data points coherently upward and downward by their systematic uncertainties. The smallest source of uncertainty is related to the systematic uncertainties of the $\rm DCA_{ee}$ templates, represented as a dashed line. The fit procedure is repeated after changing the $\rm DCA_{ee}$ resolution in the simulations used to build the templates, as well as after varying the semileptonic decay branching ratios and fragmentation functions of the charm hadrons according to their uncertainties. The former source of systematic uncertainty dominates the latter one. Finally, the statistical uncertainties of the fit, directly related to those of the data, are displayed by an ellipse. They are by far the biggest uncertainty and limit the interpretation of the results, since the data are consistent with no as well as a 65% prompt contribution in the measured dielectron yield. The larger expected data sample of Pb–Pb collisions during the LHC Run 3 and 4 periods, up to a factor 100, will allow a significant reduction of the statistical uncertainties [102–106]. At the same time, the better single-track DCA resolution of the detector, by a factor 3 and 6 in the transverse plane and in the direction of the beam axis, respectively, for Run 3 [107] and even more for Run 4 [108], will further improve the separation of prompt and non-prompt dielectron sources [109]. According to the present pioneer analysis of $\rm DCA_{ee}$, a significant extraction of QGP radiation in the IMR should be then possible in Run 3 and 4 [110].

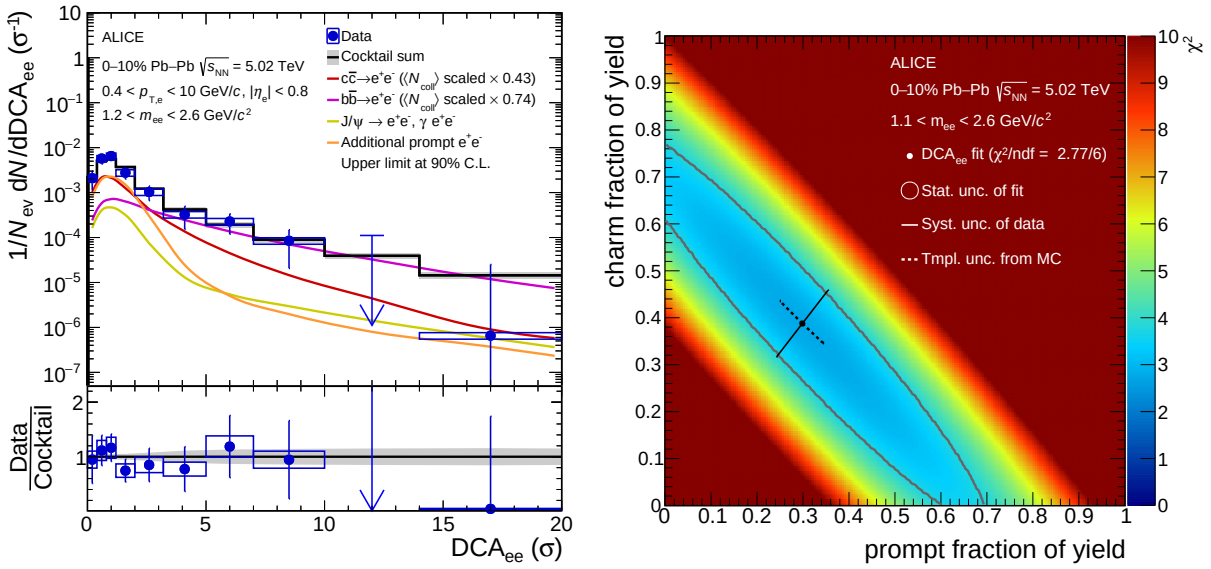

Figure 9: Left panel: fit of the inclusive e^+e^- yield in the 10% most central Pb–Pb collisions at $\sqrt{s_{\rm NN}} = 5.02$ TeV as a function of DCA_{ee} in the mass range $1.2 < m_{ee} < 2.6$ GeV/c^2. Right panel: corresponding χ^2 as a function of the two fit parameters, i.e. the ratio of the yield of e^+e^- pairs originating from a prompt source or from open-charm hadron decays to the measured e^+e^- yield. See text for more details.

7 Direct-photon production

7.1 Inclusive to decay photon ratio

In the quasi-real virtual-photon region where the $p_{\rm T,ee}$ of the dilepton pair is much larger than its mass ($p^2_{\rm T,ee} \gg m^2_{\rm ee}$), the fraction of virtual direct photons over inclusive photons can be extracted from the measured dielectron yield. To this end, the $m_{\rm ee}$ spectra in different $p_{\rm T,ee}$ intervals are fitted in the range $0.12 < m_{\rm ee} < 0.34$ GeV/c^2 with a three-component function

$$f(m_{\rm ee}) = r f_{\rm dir}(m_{\rm ee}) + (1-r) f_{\rm LF}(m_{\rm ee}) + f_{\rm HF}(m_{\rm ee}). \tag{9}$$

In the above equation, $f_{\rm dir}(m_{\rm ee})$ is the expected invariant-mass distribution of virtual direct photons, described by the Kroll–Wada equation [111], and $f_{\rm LF}(m_{\rm ee})$ and $f_{\rm HF}(m_{\rm ee})$ are the mass distributions of the light-flavor contributions without ρ and the heavy-flavor components of the hadronic cocktail, respectively. The $R_{\rm AA}^{\rm c,b\to e^\pm}$-modified HF cocktail is used for this purpose. Both $f_{\rm LF}(m_{\rm ee})$ and $f_{\rm dir}(m_{\rm ee})$ are independently normalized to the data in the mass range $0 < m_{\rm ee} < 0.03$ GeV/c^2, whereas $f_{\rm HF}(m_{\rm ee})$ is normalized accordingly to the hadronic cocktail. The only fit parameter r represents the fraction of virtual direct photons at vanishing mass, directly related to the one of real direct photons:

$$r = \left(\frac{\gamma^*_{\rm dir}}{\gamma^*_{\rm inclusive}}\right)_{m_{\rm ee}\to 0} = \left(\frac{\gamma_{\rm dir}}{\gamma_{\rm inclusive}}\right). \tag{10}$$

This approach has the advantage that the background of photons originating from hadronic decays, dominated by π^0 decays, can be suppressed by selecting e^+e^- pairs with sufficiently large $m_{\rm ee}$ ($m_{\rm ee} > m_{\pi^0}$). However, the internal conversion probability is small ($\approx 10^{-2}$) and the dielectron yield decreases rapidly as a function of $m_{\rm ee}$ ($\propto 1/m_{\rm ee}$). The fit of the measured $m_{\rm ee}$-differential dielectron yield in the $p_{\rm T,ee}$ range $1 < p_{\rm T,ee} < 2$ GeV/c is shown in the left panel of Fig. 10, together with its individual contributions.

Systematic uncertainties arise from the data, the hadronic cocktail components and the choice of the normalization and fit ranges. They are estimated in a similar way as in Refs. [53, 70, 112]. On the one

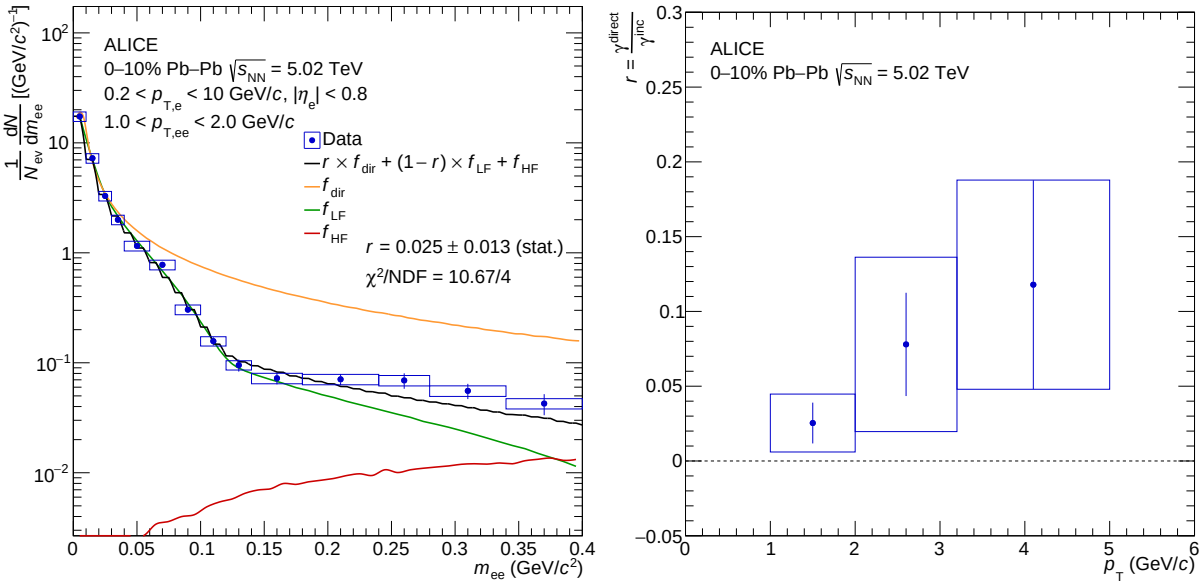

Figure 10: Left panel: fit of the dielectron yield with the three-component function defined by Eq. 10 in the 10% most central Pb–Pb collisions at $\sqrt{s_{\rm NN}} = 5.02$ TeV as a function of $m_{\rm ee}$ in the $p_{\rm T,ee}$ range $1 < p_{\rm T,ee} < 2$ GeV/c. Right panel: ratio of direct to inclusive photon yields extracted from the dielectron spectra as a function of $p_{\rm T}$ in central Pb–Pb collisions at $\sqrt{s_{\rm NN}} = 5.02$ TeV. Statistical and systematic uncertainties on the data are shown separately as vertical bars and boxes, respectively.

hand, the uncertainties from the data are evaluated by shifting all data points coherently to their upper and lower systematic uncertainties and by repeating the fit procedure. On the other hand, the different contributions of the cocktail are shifted separately according to their respective uncertainties. The limited knowledge of the η/π^0 ratio dominates the systematic uncertainties for the first $p_{\rm T,ee}$ interval, whereas the choice of the fit range becomes relevant with increasing $p_{\rm T,ee}$. The latter is estimated by varying the lower bound of the fit, keeping the upper one fixed to assure the $p^2_{\rm T,ee} \gg m^2_{\rm ee}$ condition and avoid a significant contribution from ρ hadron decays. The total systematic uncertainties on r are obtained by summing in quadrature all individual contributions and are ranging from 77% to 60% from low to high $p_{\rm T}$.

The ratio of direct to inclusive photons (r) measured in the 10% most central Pb–Pb collisions is shown as a function of $p_{\rm T}$ ($= p_{\rm T,ee}$) in the right panel of Fig. 10. The data differ from zero suggesting a source of photons that is not originating from hadronic decays. The significance of a direct photon signal is ranging from 1.07 to 1.2σ from the low to high $p_{\rm T}$ interval for virtual photons.

7.2 Direct-photon $p_{\rm T}$ spectrum

The $p_{\rm T}$-differential invariant yield of direct photons can be obtained from r and the inclusive photon yield ($\frac{{\rm d}N^{\rm incl}_{\gamma}}{{\rm d}p_{\rm T}}$). The latter is determined for each $p_{\rm T}$ interval from the yield of low mass e^+e^- pairs in the range $m_{\rm ee} < 30$ MeV/c^2 ($\frac{{\rm d}N^{\rm data}_{\rm ee}}{{\rm d}p_{\rm T}}$) following the approach used by the PHENIX collaboration [41]. The relation between real photon production and the associated e^+e^- production becomes process independent for very low $m_{\rm ee}$ (within a few percent for $m_{\rm ee} < 30$ MeV/c^2). The ratio of the expected yield of real photons from known hadronic decays ($\frac{{\rm d}N^{\rm cocktail}_{\gamma}}{{\rm d}p_{\rm T}}$) to the one of dielectrons from the same hadronic sources for $m_{\rm ee} < 30$ MeV/c^2 ($\frac{{\rm d}N^{\rm cocktail}_{\rm ee}}{{\rm d}p_{\rm T}}$) can be then used to estimate the inclusive real photon yield from the

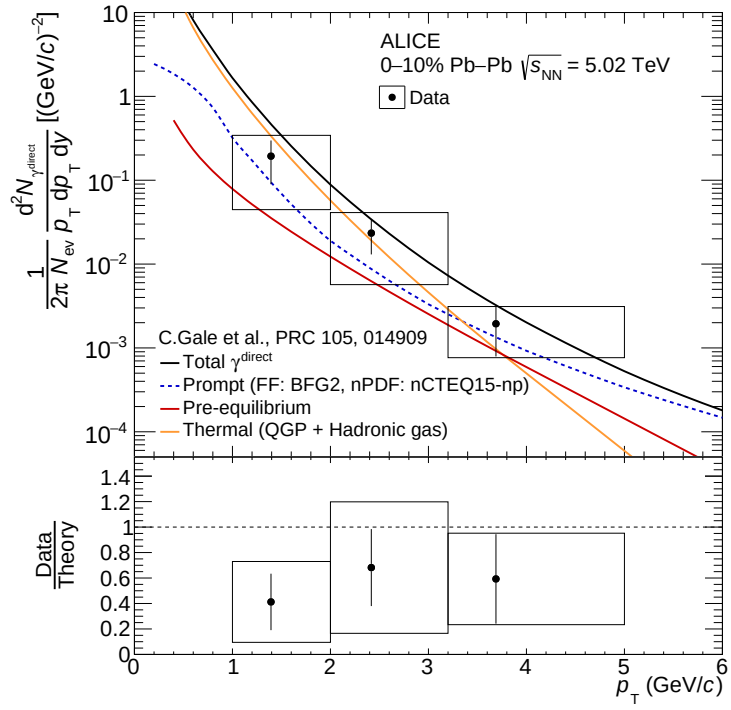

Figure 11: Direct-photon invariant yield in the 10% most central Pb–Pb collisions at $\sqrt{s_{\rm NN}} = 5.02$ TeV, compared with the predictions from a state-of-the-art model [13]. The error bars and boxes represent the statistical and systematic uncertainties of the data, respectively.

dielectron yield at low $m_{\rm ee}$, i.e.

$$\frac{{\rm d}N_\gamma^{\rm incl}}{{\rm d}p_{\rm T}} = \frac{{\rm d}N_{\rm ee}^{\rm data}}{{\rm d}p_{\rm T}} \times \left(\frac{{\rm d}N_\gamma^{\rm cocktail}}{{\rm d}p_{\rm T}} \Big/ \frac{{\rm d}N_{\rm ee}^{\rm cocktail}}{{\rm d}p_{\rm T}} \right). \tag{11}$$

Most of the uncertainties related to the parameterized $p_{\rm T}$ spectra used as input for the cocktail calculations cancel in the cocktail ratio. The resulting direct-photon $p_{\rm T}$-differential spectrum in the 10% most central Pb–Pb collisions at $\sqrt{s_{\rm NN}} = 5.02$ TeV is shown in Fig. 11. Within each $p_{\rm T}$ bin, the mean $p_{\rm T}$ is calculated with an iterative procedure using an exponential function to interpolate the $p_{\rm T}$ spectrum [113]. The data are compared to a hybrid model that describes all stages of the heavy-ion collisions [13]. The calculations include the contribution from prompt photons computed with next-to-leading-order perturbative QCD using INCNLO [114], nCTEQ15 parton distribution functions corrected for nuclear matter effects [115], and BFG-II fragmentation functions [116]. The measured direct-photon invariant yield is consistent with the prompt photon contribution alone, but the central values of the data points are systematically higher. The model predicts additional contributions from the pre-equilibrium, as well as fluid-dynamical, phases. The very early nuclear medium is described using the IP-Glasma model [117, 118] with a time-evolution determined by Yang–Mills equations. It is followed by an out-of-equilibrium phase where the energy-momentum tensor is evolved with non-equilibrium linear response functions [119, 120]. This pre-hydrodynamical K∅MP∅ST [120] phase feeds into a fluid-dynamical evolution, modelled with MUSIC [121]. The contribution of thermal photons is obtained by integrating photon emission rates over the entire space-time volume occupied by the fluid-dynamical phase. Thermal photons are the largest source of direct photons at $p_{\rm T} < 3$ GeV/c, whereas the pre-equilibrium contribution never dominates, but exceeds the thermal contribution for $p_{\rm T} > 3.5$ GeV/c. The predicted invariant yield of all direct-photon contributions together can describe the measurement, although it tends to overestimate the data by about 1σ.

7.3 Charged-particle multiplicity dependence of direct-photon production

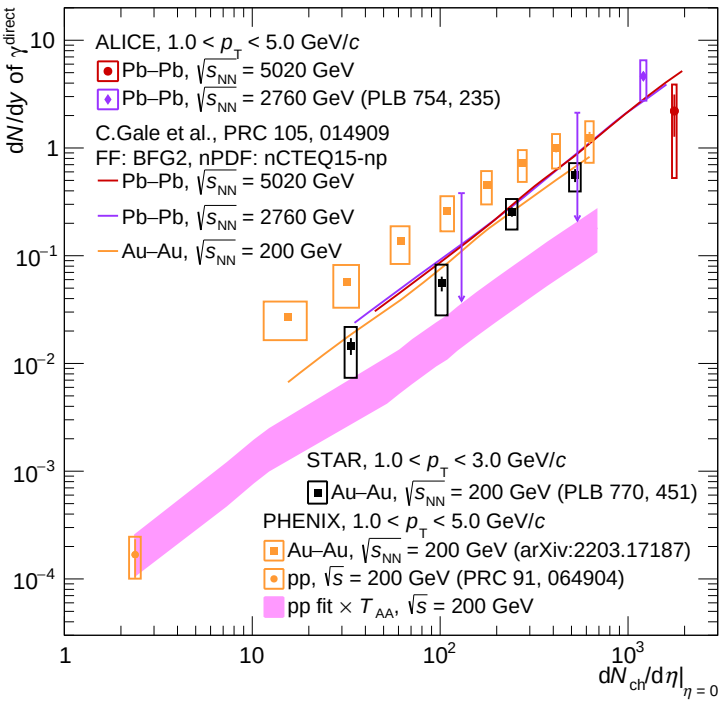

Figure 12: Integrated direct-photon yield in the $p_{\rm T}$ range $1 < p_{\rm T} < 5$ GeV/c (or $1 < p_{\rm T} < 3$ GeV/c) in Pb–Pb collisions at $\sqrt{s_{\rm NN}} = 5.02$ TeV and $\sqrt{s_{\rm NN}} = 2.76$ TeV [32], in Au–Au collisions at $\sqrt{s_{\rm NN}} = 0.2$ TeV as measured by the PHENIX [19] and STAR [27] collaborations, and in pp collisions at $\sqrt{s} = 0.2$ TeV [18]. The data are compared to predictions from a state-of-the-art model [13]. The error bars and boxes represent the statistical and systematic uncertainties of the data along the y-axis, respectively. The horizontal width of the boxes shows the total uncertainty of the measured $\frac{{\rm d}N_{\rm ch}}{{\rm d}\eta}|_{\eta=0}$ [122].

The $p_{\rm T}$-integrated direct-photon yields are shown in Fig. 12 as a function of the measured charged-particle multiplicity at midrapidity [122] for Pb–Pb collisions at $\sqrt{s_{\rm NN}} = 5.02$ (this analysis) and 2.76 TeV [32], for Au–Au collisions at $\sqrt{s_{\rm NN}} = 0.2$ TeV [19, 27], as well as for pp collisions at $\sqrt{s} = 0.2$ TeV [18]. The yields are integrated over the $p_{\rm T}$ range $1 < p_{\rm T} < 5$ GeV/c, except for the STAR data where the range is $1 < p_{\rm T} < 3$ GeV/c. The systematic uncertainties are assumed fully correlated as a function of $p_{\rm T}$ for the results at $\sqrt{s_{\rm NN}} = 5.02$ TeV. The magenta band gives the integrated direct-photon yield in pp collisions at $\sqrt{s} = 0.2$ TeV, scaled by the number of binary nucleon–nucleon collisions to the corresponding $\frac{{\rm d}N_{\rm ch}}{{\rm d}\eta}|_{\eta=0}$ for Au–Au collisions at $\sqrt{s_{\rm NN}} = 0.2$ TeV. The data are compared with predictions from the same model as the one used for the $p_{\rm T}$-differential invariant yield discussed above [13]. The calculations can reproduce the measured direct-photon yields at the LHC and in central Au–Au collisions at RHIC, although they tend to slightly overestimate the observed yield at the highest charged-particle multiplicity reported here. At lower $\frac{{\rm d}N_{\rm ch}}{{\rm d}\eta}|_{\eta=0}$ ($\frac{{\rm d}N_{\rm ch}}{{\rm d}\eta}|_{\eta=0} < 300$), the predicted direct-photon yields are smaller than the measured values by the PHENIX collaboration, with a difference increasing when moving to lower multiplicity. However, the comparison between the calculations and the data reported by the STAR collaboration for the same colliding system shows a better agreement. The discrepancy between the PHENIX and STAR results remains unresolved to this day.

The PHENIX collaboration reported an approximate power-law dependence on $\frac{{\rm d}N_{\rm ch}}{{\rm d}\eta}|_{\eta=0}$ of the direct-photon yields at low $p_{\rm T}$, with a power α independent of centrality or collision energy and similar to what would correspond to a scaling with the number of binary nucleon–nucleon collisions ($\alpha = 1.25 \pm 0.02$) shown with the magenta band in Fig. 12. However, the extracted value of α from the latest PHENIX

Au–Au data presented here is smaller than 1.25, i.e. $\alpha = 1.11 \pm 0.02$ (stat.)$^{+0.09}_{-0.08}$ (syst.) [19]. For comparison, the calculations predict α values of 1.25, 1.32 and 1.34 for Au–Au collisions at $\sqrt{s_{\rm NN}} =$ 0.2 TeV and for Pb–Pb collisions at $\sqrt{s_{\rm NN}} = 2.76$ and 5.02 TeV, respectively. The results at LHC energies are not yet sensitive to the difference between the different predicted or measured α values.

8 Summary and outlook

The first measurement at the LHC of low-mass dielectrons ($0 < m_{\rm ee} < 3.5\,{\rm GeV}/c^2$) in the 10% most central Pb–Pb collisions at $\sqrt{s_{\rm NN}} = 5.02$ TeV is presented. The $\rm e^+e^-$ pair production is measured with the ALICE detector at midrapidity ($|\eta_{\rm e}| < 0.8$) and compared with a cocktail of expected contributions from decays of known hadrons, excluding the ρ meson. The data to cocktail ratio for $0.18 < m_{\rm ee} < 0.5\,{\rm GeV}/c^2$ amounts to 1.42 ± 0.12 (stat.) ± 0.17 (syst.) ± 0.12 (cocktail) for a cocktail where the background from open heavy-flavor hadron decays is taken from dielectron measurements in pp collisions at the same center-of-mass energy per nucleon pair [90] and scaled with $N_{\rm coll}$, and 1.44 ± 0.12 (stat.) ± 0.17 (syst.)$^{+0.17}_{-0.21}$ (cocktail) for a cocktail including a modification of the heavy-flavor background based on the measured single electrons from heavy-flavor hadron decays [88] and the EPS09 nPDF [89]. The latter approach suffers from large uncertainties. The excess spectra, obtained after subtracting the hadronic cocktails, are consistent with predictions from two models that include thermal radiation from the partonic and hadronic phases [36, 99], the latter being dominant in the $m_{\rm ee}$ range considered ($0.2 < m_{\rm ee} < 0.7$ GeV$/c^2$). The uncertainties of the data do not allow the extraction of a significant thermal signal. A different method, based on the pair transverse impact parameter of the $\rm e^+e^-$ pairs, is used for the first time in Pb–Pb collisions to disentangle displaced dielectrons from heavy-flavor hadron decays from a prompt thermal contribution. The data are found to be consistent with a large suppression of $\rm e^+e^-$ pairs from $\rm c\bar{c}$, larger than for $\rm e^+e^-$ pairs from $\rm b\bar{b}$, and an additional prompt component in the intermediate-mass range ($1.2 < m_{\rm ee} < 2.6$ GeV$/c^2$), where thermal radiation from the QGP is predicted [36, 99]. The small systematic uncertainties of the results, limited by the statistical precision of the data, show the potential of such an approach for future ALICE dielectron studies with the upgraded LHC and ALICE detector, for which a significant increase of the pointing detector resolution, as well as of the size of the data sample, are expected [110]. In the quasi-real virtual-photon region ($m_{\rm ee} < 0.34$ GeV$/c^2$ and $1 < p_{\rm T,ee} < 5$ GeV$/c$), the fraction of direct photons over inclusive photons is obtained from a fit of the $m_{\rm ee}$ spectra above the π^0 mass. Combined with the inclusive real-photon yield estimated from the inclusive dielectron yield at very low $m_{\rm ee}$, the first direct-photon measurement in the 10% most central Pb–Pb collisions at $\sqrt{s_{\rm NN}} = 5.02$ TeV is reported. A model [13] including prompt photons, as well as photons from the pre-equilibrium and fluid-dynamical (thermal photons) phases can reproduce the results, while being at the upper edge of the data uncertainties.

Acknowledgements

The ALICE Collaboration would like to thank all its engineers and technicians for their invaluable contributions to the construction of the experiment and the CERN accelerator teams for the outstanding performance of the LHC complex. The ALICE Collaboration gratefully acknowledges the resources and support provided by all Grid centres and the Worldwide LHC Computing Grid (WLCG) collaboration. The ALICE Collaboration acknowledges the following funding agencies for their support in building and running the ALICE detector: A. I. Alikhanyan National Science Laboratory (Yerevan Physics Institute) Foundation (ANSL), State Committee of Science and World Federation of Scientists (WFS), Armenia; Austrian Academy of Sciences, Austrian Science Fund (FWF): [M 2467-N36] and Nationalstiftung für Forschung, Technologie und Entwicklung, Austria; Ministry of Communications and High Technologies, National Nuclear Research Center, Azerbaijan; Conselho Nacional de Desenvolvimento Científico e Tecnológico (CNPq), Financiadora de Estudos e Projetos (Finep), Fundação de Amparo à Pesquisa do Estado de São Paulo (FAPESP) and Universidade Federal do Rio Grande do Sul (UFRGS),

Brazil; Bulgarian Ministry of Education and Science, within the National Roadmap for Research Infrastructures 2020-2027 (object CERN), Bulgaria; Ministry of Education of China (MOEC) , Ministry of Science & Technology of China (MSTC) and National Natural Science Foundation of China (NSFC), China; Ministry of Science and Education and Croatian Science Foundation, Croatia; Centro de Aplicaciones Tecnológicas y Desarrollo Nuclear (CEADEN), Cubaenergía, Cuba; Ministry of Education, Youth and Sports of the Czech Republic, Czech Republic; The Danish Council for Independent Research | Natural Sciences, the VILLUM FONDEN and Danish National Research Foundation (DNRF), Denmark; Helsinki Institute of Physics (HIP), Finland; Commissariat à l'Energie Atomique (CEA) and Institut National de Physique Nucléaire et de Physique des Particules (IN2P3) and Centre National de la Recherche Scientifique (CNRS), France; Bundesministerium für Bildung und Forschung (BMBF) and GSI Helmholtzzentrum für Schwerionenforschung GmbH, Germany; General Secretariat for Research and Technology, Ministry of Education, Research and Religions, Greece; National Research, Development and Innovation Office, Hungary; Department of Atomic Energy Government of India (DAE), Department of Science and Technology, Government of India (DST), University Grants Commission, Government of India (UGC) and Council of Scientific and Industrial Research (CSIR), India; National Research and Innovation Agency - BRIN, Indonesia; Istituto Nazionale di Fisica Nucleare (INFN), Italy; Japanese Ministry of Education, Culture, Sports, Science and Technology (MEXT) and Japan Society for the Promotion of Science (JSPS) KAKENHI, Japan; Consejo Nacional de Ciencia (CONACYT) y Tecnología, through Fondo de Cooperación Internacional en Ciencia y Tecnología (FONCICYT) and Dirección General de Asuntos del Personal Academico (DGAPA), Mexico; Nederlandse Organisatie voor Wetenschappelijk Onderzoek (NWO), Netherlands; The Research Council of Norway, Norway; Commission on Science and Technology for Sustainable Development in the South (COMSATS), Pakistan; Pontificia Universidad Católica del Perú, Peru; Ministry of Education and Science, National Science Centre and WUT ID-UB, Poland; Korea Institute of Science and Technology Information and National Research Foundation of Korea (NRF), Republic of Korea; Ministry of Education and Scientific Research, Institute of Atomic Physics, Ministry of Research and Innovation and Institute of Atomic Physics and University Politehnica of Bucharest, Romania; Ministry of Education, Science, Research and Sport of the Slovak Republic, Slovakia; National Research Foundation of South Africa, South Africa; Swedish Research Council (VR) and Knut & Alice Wallenberg Foundation (KAW), Sweden; European Organization for Nuclear Research, Switzerland; Suranaree University of Technology (SUT), National Science and Technology Development Agency (NSTDA) and National Science, Research and Innovation Fund (NSRF via PMU-B B05F650021), Thailand; Turkish Energy, Nuclear and Mineral Research Agency (TENMAK), Turkey; National Academy of Sciences of Ukraine, Ukraine; Science and Technology Facilities Council (STFC), United Kingdom; National Science Foundation of the United States of America (NSF) and United States Department of Energy, Office of Nuclear Physics (DOE NP), United States of America. In addition, individual groups or members have received support from: European Research Council, Strong 2020 - Horizon 2020 (grant nos. 950692, 824093), European Union; Academy of Finland (Center of Excellence in Quark Matter) (grant nos. 346327, 346328), Finland.

References

[1] **ALICE** Collaboration, "The ALICE experiment – A journey through QCD", arXiv:2211.04384 [nucl-ex].

[2] A. Bazavov *et al.*, "The chiral and deconfinement aspects of the QCD transition", *Phys. Rev. D* **85** (2012) 054503, arXiv:1111.1710 [hep-lat].

[3] S. Borsanyi, Z. Fodor, C. Hoelbling, S. D. Katz, S. Krieg, and K. K. Szabo, "Full result for the QCD equation of state with 2+1 flavors", *Phys. Lett. B* **730** (2014) 99–104, arXiv:1309.5258 [hep-lat].

[4] **HotQCD** Collaboration, A. Bazavov *et al.*, "Chiral crossover in QCD at zero and non-zero chemical potentials", *Phys. Lett. B* **795** (2019) 15–21, arXiv:1812.08235 [hep-lat].

[5] S. Borsanyi, Z. Fodor, J. N. Guenther, R. Kara, S. D. Katz, P. Parotto, A. Pasztor, C. Ratti, and K. K. Szabo, "QCD Crossover at Finite Chemical Potential from Lattice Simulations", *Phys. Rev. Lett.* **125** (2020) 052001, arXiv:2002.02821 [hep-lat].

[6] N. Bilic and H. Nikolic, "Chiral symmetry restoration in the linear sigma model at nonzero temperature and baryon density", *Eur. Phys. J. C* **6** (1999) 515–523, arXiv:hep-ph/9711513.

[7] C. A. Dominguez, M. Loewe, and Y. Zhang, "Chiral symmetry restoration and deconfinement in QCD at finite temperature", *Phys. Rev. D* **86** (2012) 034030, arXiv:1205.3361 [hep-ph]. [Erratum: Phys.Rev.D 90, 039903 (2014)].

[8] C. Gale, "Photon Production in Hot and Dense Strongly Interacting Matter", *Landolt-Bornstein* **23** (2010) 445, arXiv:0904.2184 [hep-ph].

[9] S. Turbide, C. Gale, S. Jeon, and G. D. Moore, "Energy loss of leading hadrons and direct photon production in evolving quark-gluon plasma", *Phys. Rev. C* **72** (2005) 014906, arXiv:hep-ph/0502248.

[10] G.-Y. Qin, J. Ruppert, C. Gale, S. Jeon, and G. D. Moore, "Jet energy loss, photon production, and photon-hadron correlations at RHIC", *Phys. Rev. C* **80** (2009) 054909, arXiv:0906.3280 [hep-ph].

[11] J. I. Kapusta, P. Lichard, and D. Seibert, "High-energy photons from quark-gluon plasma versus hot hadronic gas", *Phys. Rev. D* **44** (1991) 2774–2788. [Erratum: Phys.Rev.D 47, 4171 (1993)].

[12] S. Turbide, R. Rapp, and C. Gale, "Hadronic production of thermal photons", *Phys. Rev. C* **69** (2004) 014903, arXiv:hep-ph/0308085.

[13] C. Gale, J.-F. Paquet, B. Schenke, and C. Shen, "Multimessenger heavy-ion collision physics", *Phys. Rev. C* **105** (2022) 014909, arXiv:2106.11216 [nucl-th].

[14] **WA98** Collaboration, M. M. Aggarwal *et al.*, "Observation of direct photons in central 158-A-GeV Pb-208 + Pb-208 collisions", *Phys. Rev. Lett.* **85** (2000) 3595–3599, arXiv:nucl-ex/0006008.

[15] **PHENIX** Collaboration, S. S. Adler *et al.*, "Centrality dependence of direct photon production in $\sqrt{s_{\rm NN}} = 200$ GeV Au+Au collisions", *Phys. Rev. Lett.* **94** (2005) 232301, arXiv:nucl-ex/0503003.

[16] **PHENIX** Collaboration, A. Adare *et al.*, "Enhanced production of direct photons in Au+Au collisions at $\sqrt{s_{\rm NN}} = 200$ GeV and implications for the initial temperature", *Phys. Rev. Lett.* **104** (2010) 132301, arXiv:0804.4168 [nucl-ex].

[17] **PHENIX** Collaboration, A. Adare *et al.*, "Observation of direct-photon collective flow in $\sqrt{s_{\rm NN}} = 200$ GeV Au+Au collisions", *Phys. Rev. Lett.* **109** (2012) 122302, arXiv:1105.4126 [nucl-ex].

[18] **PHENIX** Collaboration, A. Adare *et al.*, "Centrality dependence of low-momentum direct-photon production in Au+Au collisions at $\sqrt{s_{\rm NN}} = 200$ GeV", *Phys. Rev. C* **91** (2015) 064904, arXiv:1405.3940 [nucl-ex].

[19] **PHENIX** Collaboration, U. A. Acharya *et al.*, "Nonprompt direct-photon production in Au+Au collisions at $\sqrt{s_{\rm NN}} = 200$ GeV", arXiv:2203.17187 [nucl-ex].

[20] **PHENIX** Collaboration, A. Adare *et al.*, "Azimuthally anisotropic emission of low-momentum direct photons in Au+Au collisions at $\sqrt{s_{\rm NN}} = 200$ GeV", *Phys. Rev. C* **94** (2016) 064901, arXiv:1509.07758 [nucl-ex].

[21] **PHENIX** Collaboration, A. Adare *et al.*, "Beam Energy and Centrality Dependence of Direct-Photon Emission from Ultrarelativistic Heavy-Ion Collisions", *Phys. Rev. Lett.* **123** (2019) 022301, arXiv:1805.04084 [hep-ex].

[22] **PHENIX** Collaboration, N. J. Abdulameer *et al.*, "Low-pT direct-photon production in Au+Au collisions at $\sqrt{s_{\rm NN}} = 39$ and 62.4 GeV", *Phys. Rev. C* **107** (2023) 024914, arXiv:2203.12354 [nucl-ex].

[23] **PHENIX** Collaboration, S. S. Adler *et al.*, "Measurement of direct photon production in $p+p$ collisions $\sqrt{s} = 200$ GeV", *Phys. Rev. Lett.* **98** (2007) 012002, arXiv:hep-ex/0609031.

[24] **PHENIX** Collaboration, A. Adare *et al.*, "Direct-Photon Production in $p+p$ Collisions at $\sqrt{s} = 200$ GeV at Midrapidity", *Phys. Rev. D* **86** (2012) 072008, arXiv:1205.5533 [hep-ex].

[25] **PHENIX** Collaboration, A. Adare *et al.*, "Direct photon production in d+Au collisions at $\sqrt{s_{\rm NN}} = 200$ GeV", *Phys. Rev. C* **87** (2013) 054907, arXiv:1208.1234 [nucl-ex].

[26] J.-F. Paquet, C. Shen, G. S. Denicol, M. Luzum, B. Schenke, S. Jeon, and C. Gale, "Production of photons in relativistic heavy-ion collisions", *Phys. Rev. C* **93** (2016) 044906, arXiv:1509.06738 [hep-ph].

[27] **STAR** Collaboration, L. Adamczyk *et al.*, "Direct virtual photon production in Au+Au collisions at $\sqrt{s_{\rm NN}} = 200$ GeV", *Phys. Lett. B* **770** (2017) 451–458, arXiv:1607.01447 [nucl-ex].

[28] R. Chatterjee, H. Holopainen, I. Helenius, T. Renk, and K. J. Eskola, "Elliptic flow of thermal photons from event-by-event hydrodynamic model", *Phys. Rev. C* **88** (2013) 034901, arXiv:1305.6443 [hep-ph].

[29] C. Gale, Y. Hidaka, S. Jeon, S. Lin, J.-F. Paquet, R. D. Pisarski, D. Satow, V. V. Skokov, and G. Vujanovic, "Production and Elliptic Flow of Dileptons and Photons in a Matrix Model of the Quark-Gluon Plasma", *Phys. Rev. Lett.* **114** (2015) 072301, arXiv:1409.4778 [hep-ph].

[30] R. Chatterjee, P. Dasgupta, and D. K. Srivastava, "Anisotropic flow of thermal photons at energies available at the BNL Relativistic Heavy Ion Collider and at the CERN Large Hadron Collider", *Phys. Rev. C* **96** (2017) 014911, arXiv:1702.02378 [nucl-th].

[31] O. Linnyk, V. Konchakovski, T. Steinert, W. Cassing, and E. L. Bratkovskaya, "Hadronic and partonic sources of direct photons in relativistic heavy-ion collisions", *Phys. Rev. C* **92** (2015) 054914, arXiv:1504.05699 [nucl-th].

[32] **ALICE** Collaboration, J. Adam *et al.*, "Direct photon production in Pb–Pb collisions at $\sqrt{s_{\rm NN}} =$ 2.76 TeV", *Phys. Lett. B* **754** (2016) 235–248, arXiv:1509.07324 [nucl-ex].

[33] **ALICE** Collaboration, S. Acharya *et al.*, "Direct photon elliptic flow in Pb–Pb collisions at $\sqrt{s_{\rm NN}}$ = 2.76 TeV", *Phys. Lett. B* **789** (2019) 308–322, arXiv:1805.04403 [nucl-ex].

[34] C. Shen, U. W. Heinz, J.-F. Paquet, and C. Gale, "Thermal photons as a quark-gluon plasma thermometer reexamined", *Phys. Rev. C* **89** (2014) 044910, arXiv:1308.2440 [nucl-th].

[35] R. Rapp and H. van Hees, "Thermal Dileptons as Fireball Thermometer and Chronometer", *Phys. Lett. B* **753** (2016) 586–590, arXiv:1411.4612 [hep-ph].

[36] R. Rapp, "Dilepton Spectroscopy of QCD Matter at Collider Energies", *Adv. High Energy Phys.* **2013** (2013) 148253, arXiv:1304.2309 [hep-ph].

[37] M. Coquet, X. Du, J.-Y. Ollitrault, S. Schlichting, and M. Winn, "Intermediate mass dileptons as pre-equilibrium probes in heavy ion collisions", *Phys. Lett. B* **821** (2021) 136626, arXiv:2104.07622 [nucl-th].

[38] M. Coquet, X. Du, J.-Y. Ollitrault, S. Schlichting, and M. Winn, "Transverse mass scaling of dilepton radiation off a quark-gluon plasma", *Nucl. Phys. A* **1030** (2023) 122579, arXiv:2112.13876 [nucl-th].

[39] R. D. Pisarski, "Where does the ρ go? Chirally symmetric vector mesons in the quark-gluon plasma", *Phys. Rev. D* **52** (1995) R3773–R3776, arXiv:hep-ph/9503328.

[40] P. M. Hohler and R. Rapp, "Is ρ-Meson Melting Compatible with Chiral Restoration?", *Phys. Lett. B* **731** (2014) 103–109, arXiv:1311.2921 [hep-ph].

[41] **PHENIX** Collaboration, A. Adare *et al.*, "Detailed measurement of the e^+e^- pair continuum in $p+p$ and Au+Au collisions at $\sqrt{s_{NN}} = 200$ GeV and implications for direct photon production", *Phys. Rev. C* **81** (2010) 034911, arXiv:0912.0244 [nucl-ex].

[42] **CERES/NA45** Collaboration, G. Agakichiev *et al.*, "Low mass e^+e^- pair production in 158/A-GeV Pb-Au collisions at the CERN SPS, its dependence on multiplicity and transverse momentum", *Phys. Lett. B* **422** (1998) 405–412, arXiv:nucl-ex/9712008.

[43] **CERES/NA45** Collaboration, D. Adamova *et al.*, "Enhanced production of low mass electron pairs in 40-AGeV Pb-Au collisions at the CERN SPS", *Phys. Rev. Lett.* **91** (2003) 042301, arXiv:nucl-ex/0209024.

[44] **CERES** Collaboration, D. Adamova *et al.*, "Modification of the ρ-meson detected by low-mass electron-positron pairs in central Pb-Au collisions at 158-A-GeV/c", *Phys. Lett. B* **666** (2008) 425–429, arXiv:nucl-ex/0611022.

[45] **NA60** Collaboration, R. Arnaldi *et al.*, "Evidence for the production of thermal-like muon pairs with masses above 1 GeV/c^2 in 158-A-GeV Indium-Indium Collisions", *Eur. Phys. J. C* **59** (2009) 607–623, arXiv:0810.3204 [nucl-ex].

[46] **NA60** Collaboration, R. Arnaldi *et al.*, "First measurement of the ρ spectral function in high-energy nuclear collisions", *Phys. Rev. Lett.* **96** (2006) 162302, arXiv:nucl-ex/0605007.

[47] **NA60** Collaboration, R. Arnaldi *et al.*, "NA60 results on thermal dimuons", *Eur. Phys. J. C* **61** (2009) 711–720, arXiv:0812.3053 [nucl-ex].

[48] **NA60** Collaboration, H. J. Specht, "Thermal Dileptons from Hot and Dense Strongly Interacting Matter", *AIP Conf. Proc.* **1322** (2010) 1–10, arXiv:1011.0615 [nucl-ex].

[49] T. Renk and J. Ruppert, "Dimuon transverse momentum spectra as a tool to characterize the emission region in heavy-ion collisions", *Phys. Rev. C* **77** (2008) 024907, arXiv:hep-ph/0612113.

[50] J. Ruppert, C. Gale, T. Renk, P. Lichard, and J. I. Kapusta, "Low mass dimuons produced in relativistic nuclear collisions", *Phys. Rev. Lett.* **100** (2008) 162301, arXiv:0706.1934 [hep-ph].

[51] **PHENIX** Collaboration, A. Adare *et al.*, "Dielectron production in Au+Au collisions at $\sqrt{s_{NN}}$=200 GeV", *Phys. Rev. C* **93** (2016) 014904, arXiv:1509.04667 [nucl-ex].

[52] **STAR** Collaboration, L. Adamczyk *et al.*, "Dielectron Mass Spectra from Au+Au Collisions at $\sqrt{s_{\rm NN}}$ = 200 GeV", *Phys. Rev. Lett.* **113** (2014) 022301, arXiv:1312.7397 [hep-ex]. [Addendum: Phys.Rev.Lett. 113, 049903 (2014)].

[53] **ALICE** Collaboration, S. Acharya *et al.*, "Measurement of dielectron production in central Pb–Pb collisions at $\sqrt{s_{\rm NN}}$ = 2.76 TeV", *Phys. Rev. C* **99** (2019) 024002, arXiv:1807.00923 [nucl-ex].

[54] R. Rapp and J. Wambach, "Low mass dileptons at the CERN SPS: Evidence for chiral restoration?", *Eur. Phys. J. A* **6** (1999) 415–420, arXiv:hep-ph/9907502.

[55] H. van Hees and R. Rapp, "Dilepton Radiation at the CERN Super Proton Synchrotron", *Nucl. Phys. A* **806** (2008) 339–387, arXiv:0711.3444 [hep-ph].

[56] R. Rapp, "Signatures of thermal dilepton radiation at RHIC", *Phys. Rev. C* **63** (2001) 054907, arXiv:hep-ph/0010101.

[57] O. Linnyk, W. Cassing, J. Manninen, E. L. Bratkovskaya, and C. M. Ko, "Analysis of dilepton production in Au+Au collisions at $\sqrt{s_{NN}} = 200$ GeV within the Parton-Hadron-String Dynamics (PHSD) transport approach", *Phys. Rev. C* **85** (2012) 024910, arXiv:1111.2975 [nucl-th].

[58] **ALICE** Collaboration, K. Aamodt *et al.*, "The ALICE experiment at the CERN LHC", *JINST* **3** (2008) S08002.

[59] **ALICE** Collaboration, B. Abelev *et al.*, "Performance of the ALICE Experiment at the CERN LHC", *Int. J. Mod. Phys. A* **29** (2014) 1430044, arXiv:1402.4476 [nucl-ex].

[60] **ALICE** Collaboration, K. Aamodt *et al.*, "Alignment of the ALICE Inner Tracking System with cosmic-ray tracks", *JINST* **5** (2010) P03003, arXiv:1001.0502 [physics.ins-det].

[61] J. Alme *et al.*, "The ALICE TPC, a large 3-dimensional tracking device with fast readout for ultra-high multiplicity events", *Nucl. Instrum. Meth. A* **622** (2010) 316–367, arXiv:1001.1950 [physics.ins-det].

[62] A. Akindinov *et al.*, "Performance of the ALICE Time-Of-Flight detector at the LHC", *Eur. Phys. J. Plus* **128** (2013) 44.

[63] **ALICE** Collaboration, E. Abbas *et al.*, "Performance of the ALICE VZERO system", *JINST* **8** (2013) P10016, arXiv:1306.3130 [nucl-ex].

[64] R. Arnaldi *et al.*, "The Zero degree calorimeters for the ALICE experiment", *Nucl. Instrum. Meth. A* **581** (2007) 397–401. [Erratum: Nucl.Instrum.Meth.A 604, 765 (2009)].

[65] **ALICE** Collaboration, "Centrality determination in heavy ion collisions", *ALICE-PUBLIC-2018-011* (2018) . http://cds.cern.ch/record/2636623.

[66] **ALICE** Collaboration, "ALICE luminosity determination for Pb−Pb collisions at $\sqrt{s_{\rm NN}} = 5.02$ TeV", arXiv:2204.10148 [nucl-ex].

[67] **ALICE** Collaboration, S. Acharya *et al.*, "Data-driven precision determination of the material budget in ALICE", arXiv:2303.15317 [physics.ins-det].

[68] **ALICE** Collaboration, S. Acharya *et al.*, "Dielectron production at midrapidity at low transverse momentum in peripheral and semi-peripheral Pb–Pb collisions at $\sqrt{s_{\rm NN}}$ = 5.02 TeV", *JHEP* **06** (2023) 024, arXiv:2204.11732 [nucl-ex].

[69] **NA60** Collaboration, R. Shahoyan, "Evidence for the production of thermal dimuons with masses above 1-GeV/c**2 in 158A-GeV In-In collisions", *Nucl. Phys. A* **827** (2009) 353C–355C.

[70] **ALICE** Collaboration, S. Acharya *et al.*, "Dielectron production in proton–proton collisions at $\sqrt{s} = 7$ TeV", *JHEP* **09** (2018) 064, arXiv:1805.04391 [hep-ex].

[71] R. Brun, F. Bruyant, M. Maire, A. C. McPherson, and P. Zanarini, *GEANT 3: user's guide Geant 3.10, Geant 3.11; rev. version*. CERN, Geneva, 1987. https://cds.cern.ch/record/1119728.

[72] X.-N. Wang and M. Gyulassy, "HIJING: A Monte Carlo model for multiple jet production in p p, p A and A A collisions", *Phys. Rev. D* **44** (1991) 3501–3516.

[73] P. Golonka and Z. Was, "PHOTOS Monte Carlo: A Precision tool for QED corrections in Z and W decays", *Eur. Phys. J. C* **45** (2006) 97–107, arXiv:hep-ph/0506026.

[74] P. Z. Skands, "Tuning Monte Carlo Generators: The Perugia Tunes", *Phys. Rev. D* **82** (2010) 074018, arXiv:1005.3457 [hep-ph].

[75] T. Sjostrand, S. Mrenna, and P. Z. Skands, "PYTHIA 6.4 Physics and Manual", *JHEP* **05** (2006) 026, arXiv:hep-ph/0603175.

[76] **ALICE** Collaboration, "Momentum transformation matrix for dielectron simulations in Pb–Pb collisions at $\sqrt{s_{\rm NN}} = 2.76$ TeV", *ALICE-PUBLIC-2017-011* (2017) . http://cds.cern.ch/record/2289779.

[77] **ALICE** Collaboration, S. Acharya *et al.*, "Production of charged pions, kaons, and (anti-)protons in Pb–Pb and inelastic pp collisions at $\sqrt{s_{NN}}$ = 5.02 TeV", *Phys. Rev. C* **101** (2020) 044907, arXiv:1910.07678 [nucl-ex].

[78] **ALICE** Collaboration, S. Acharya *et al.*, "Soft-Dielectron Excess in Proton–Proton Collisions at $\sqrt{s}$ = 13 TeV", *Phys. Rev. Lett.* **127** (2021) 042302, arXiv:2005.14522 [nucl-ex].

[79] Y. Ren and A. Drees, "Study of the η to π^0 Ratio in Heavy-Ion Collisions", *Phys. Rev. C* **104** (2021) 054902, arXiv:2102.05220 [nucl-ex].

[80] **ALICE** Collaboration, B. Abelev *et al.*, "Neutral pion and η meson production in proton–proton collisions at $\sqrt{s} = 0.9$ TeV and $\sqrt{s} = 7$ TeV", *Phys. Lett. B* **717** (2012) 162–172, arXiv:1205.5724 [hep-ex].

[81] **ALICE** Collaboration, S. Acharya *et al.*, "π^0 and η meson production in proton–proton collisions at $\sqrt{s} = 8$ TeV", *Eur. Phys. J. C* **78** (2018) 263, arXiv:1708.08745 [hep-ex].

[82] **ALICE** Collaboration, S. Acharya *et al.*, "Neutral pion and η meson production in p–Pb collisions at $\sqrt{s_{\rm NN}} = 5.02$ TeV", *Eur. Phys. J. C* **78** (2018) 624, arXiv:1801.07051 [nucl-ex].

[83] **ALICE** Collaboration, S. Acharya *et al.*, "Production of π^0 and η mesons up to high transverse momentum in pp collisions at $\sqrt{s} = 2.76$ TeV", *Eur. Phys. J. C* **77** (2017) 339, arXiv:1702.00917 [hep-ex].

[84] G. Agakichiev *et al.*, "Neutral meson production in p Be and p Au collisions at 450-GeV beam energy", *Eur. Phys. J. C* **4** (1998) 249–257.

[85] **ALICE** Collaboration, S. Acharya *et al.*, "Neutral pion and η meson production at midrapidity in Pb–Pb collisions at $\sqrt{s_{\rm NN}}$ = 2.76 TeV", *Phys. Rev. C* **98** (2018) 044901, arXiv:1803.05490 [nucl-ex].

[86] **ALICE** Collaboration, S. Acharya *et al.*, "Evidence of rescattering effect in Pb-Pb collisions at the LHC through production of $K^*(892)^0$ and $\phi(1020)$ mesons", *Phys. Lett. B* **802** (2020) 135225, arXiv:1910.14419 [nucl-ex].

[87] **ALICE** Collaboration, S. Acharya *et al.*, "Prompt and non-prompt J/ψ production at midrapidity in Pb−Pb collisions at $\sqrt{s_{\rm NN}}$ = 5.02 TeV", arXiv:2308.16125 [nucl-ex].

[88] **ALICE** Collaboration, S. Acharya *et al.*, "Measurement of electrons from semileptonic heavy-flavour hadron decays at midrapidity in pp and Pb–Pb collisions at $\sqrt{s_{\rm NN}}$ = 5.02 TeV", *Phys. Lett. B* **804** (2020) 135377, arXiv:1910.09110 [nucl-ex].

[89] K. J. Eskola, H. Paukkunen, and C. A. Salgado, "EPS09: A New Generation of NLO and LO Nuclear Parton Distribution Functions", *JHEP* **04** (2009) 065, arXiv:0902.4154 [hep-ph].

[90] **ALICE** Collaboration, S. Acharya *et al.*, "Dielectron production in proton–proton and proton–lead collisions at $\sqrt{s_{\rm NN}} = 5.02$ TeV", *Phys. Rev. C* **102** (2020) 055204, arXiv:2005.11995 [nucl-ex].

[91] P. Nason, "A New method for combining NLO QCD with shower Monte Carlo algorithms", *JHEP* **11** (2004) 040, arXiv:hep-ph/0409146 [hep-ph].

[92] S. Frixione, P. Nason, and G. Ridolfi, "A Positive-weight next-to-leading-order Monte Carlo for heavy flavour hadroproduction", *JHEP* **09** (2007) 126.

[93] S. Frixione, P. Nason, and C. Oleari, "Matching NLO QCD computations with Parton Shower simulations: the POWHEG method", *JHEP* **11** (2007) 070.

[94] S. Alioli, P. Nason, C. Oleari, and E. Re, "A general framework for implementing NLO calculations in shower Monte Carlo programs: the POWHEG BOX", *JHEP* **06** (2010) 043, arXiv:1002.2581 [hep-ph].

[95] **Particle Data Group** Collaboration, R. L. Workman *et al.*, "Review of Particle Physics", *PTEP* **2022** (2022) 083C01.

[96] **ALICE** Collaboration, S. Acharya *et al.*, "Charm-quark fragmentation fractions and production cross section at midrapidity in pp collisions at the LHC", *Phys. Rev. D* **105** (2022) L011103, arXiv:2105.06335 [nucl-ex].

[97] **ALICE** Collaboration, S. Acharya *et al.*, "Prompt D^0, D^+, and D^{*+} production in Pb–Pb collisions at $\sqrt{s_{\rm NN}}$ = 5.02 TeV", *JHEP* **01** (2022) 174, arXiv:2110.09420 [nucl-ex].

[98] **ALICE** Collaboration, S. Acharya *et al.*, "Constraining hadronization mechanisms with Λc+/D0 production ratios in Pb–Pb collisions at sNN=5.02 TeV", *Phys. Lett. B* **839** (2023) 137796, arXiv:2112.08156 [nucl-ex].

[99] T. Song, W. Cassing, P. Moreau, and E. Bratkovskaya, "Open charm and dileptons from relativistic heavy-ion collisions", *Phys. Rev. C* **97** (2018) 064907, arXiv:1803.02698 [nucl-th].

[100] G. J. Feldman and R. D. Cousins, "A Unified approach to the classical statistical analysis of small signals", *Phys. Rev. D* **57** (1998) 3873–3889, arXiv:physics/9711021.

[101] O. Linnyk, E. L. Bratkovskaya, J. Manninen, and W. Cassing, "Dilepton production from parton interactions in the early stage of relativistic heavy-ion collisions", *J. Phys. Conf. Ser.* **312** (2011) 012010, arXiv:1102.3624 [nucl-th].

[102] **ALICE** Collaboration, "Upgrade of the ALICE Time Projection Chamber", *CERN-LHCC-2013-020* (2013) . https://cds.cern.ch/record/1622286.

[103] **ALICE** Collaboration, "Addendum to the Technical Design Report for the Upgrade of the ALICE Time Projection Chamber", *CERN-LHCC-2015-002* (2015) . https://cds.cern.ch/record/1984329.

[104] **ALICE TPC** Collaboration, J. Adolfsson *et al.*, "The upgrade of the ALICE TPC with GEMs and continuous readout", *JINST* **16** (2021) P03022, arXiv:2012.09518 [physics.ins-det].

[105] **ALICE** Collaboration, P. Antonioli, A. Kluge, and W. Riegler, "Upgrade of the ALICE Readout and Trigger System", *CERN-LHCC-2013-019* (2013) . https://cds.cern.ch/record/1603472.

[106] **ALICE** Collaboration, P. Buncic, M. Krzewicki, and P. Vande Vyvre, "Technical Design Report for the Upgrade of the Online-Offline Computing System", *CERN-LHCC-2015-006* (2015) . https://cds.cern.ch/record/2011297.

[107] **ALICE** Collaboration, "Upgrade of the Inner Tracking System Conceptual Design Report. Conceptual Design Report for the Upgrade of the ALICE ITS", *CERN-LHCC-2012-013* (2012) . https://cds.cern.ch/record/1475244.

[108] **ALICE** Collaboration, "Expression of Interest for an ALICE ITS Upgrade in LS3", *ALICE-PUBLIC-2018-013* (2018) . http://cds.cern.ch/record/2644611.

[109] Z. Citron *et al.*, "Report from Working Group 5: Future physics opportunities for high-density QCD at the LHC with heavy-ion and proton beams", *CERN Yellow Rep. Monogr.* **7** (2019) 1159–1410, arXiv:1812.06772 [hep-ph].

[110] **ALICE** Collaboration, "ALICE upgrades during the LHC Long Shutdown 2", arXiv:2302.01238 [physics.ins-det].

[111] N. M. Kroll and W. Wada, "Internal pair production associated with the emission of high-energy gamma rays", *Phys. Rev.* **98** (1955) 1355–1359.

[112] **ALICE** Collaboration, S. Acharya *et al.*, "Dielectron and heavy-quark production in inelastic and high-multiplicity proton–proton collisions at $\sqrt{s_{NN}} = 13$TeV", *Phys. Lett. B* **788** (2019) 505–518, arXiv:1805.04407 [hep-ex].

[113] G. Lafferty and T. Wyatt, "Where to stick your data points: The treatment of measurements within wide bins", *Nuclear Instruments and Methods in Physics Research Section A: Accelerators, Spectrometers, Detectors and Associated Equipment* **355** (1995) 541–547. https://www.sciencedirect.com/science/article/pii/0168900294011125.

[114] P. Aurenche, M. Fontannaz, J. P. Guillet, B. A. Kniehl, E. Pilon, and M. Werlen, "A Critical phenomenological study of inclusive photon production in hadronic collisions", *Eur. Phys. J. C* **9** (1999) 107–119, arXiv:hep-ph/9811382.

[115] K. Kovarik *et al.*, "nCTEQ15 - Global analysis of nuclear parton distributions with uncertainties in the CTEQ framework", *Phys. Rev. D* **93** (2016) 085037, arXiv:1509.00792 [hep-ph].

[116] L. Bourhis, M. Fontannaz, and J. P. Guillet, "Quarks and gluon fragmentation functions into photons", *Eur. Phys. J. C* **2** (1998) 529–537, arXiv:hep-ph/9704447.

[117] B. Schenke, P. Tribedy, and R. Venugopalan, "Fluctuating Glasma initial conditions and flow in heavy ion collisions", *Phys. Rev. Lett.* **108** (2012) 252301, arXiv:1202.6646 [nucl-th].

[118] B. Schenke, P. Tribedy, and R. Venugopalan, "Event-by-event gluon multiplicity, energy density, and eccentricities in ultrarelativistic heavy-ion collisions", *Phys. Rev. C* **86** (2012) 034908, arXiv:1206.6805 [hep-ph].

[119] A. Kurkela, A. Mazeliauskas, J.-F. Paquet, S. Schlichting, and D. Teaney, "Matching the Nonequilibrium Initial Stage of Heavy Ion Collisions to Hydrodynamics with QCD Kinetic Theory", *Phys. Rev. Lett.* **122** (2019) 122302, arXiv:1805.01604 [hep-ph].

[120] A. Kurkela, A. Mazeliauskas, J.-F. Paquet, S. Schlichting, and D. Teaney, "Effective kinetic description of event-by-event pre-equilibrium dynamics in high-energy heavy-ion collisions", *Phys. Rev. C* **99** (2019) 034910, arXiv:1805.00961 [hep-ph].

[121] B. Schenke, S. Jeon, and C. Gale, "(3+1)D hydrodynamic simulation of relativistic heavy-ion collisions", *Phys. Rev. C* **82** (2010) 014903, arXiv:1004.1408 [hep-ph].

[122] **ALICE** Collaboration, J. Adam *et al.*, "Centrality Dependence of the Charged-Particle Multiplicity Density at Midrapidity in Pb-Pb Collisions at $\sqrt{s_{\rm NN}}$ = 5.02 TeV", *Phys. Rev. Lett.* **116** (2016) 222302, arXiv:1512.06104 [nucl-ex].

A The ALICE Collaboration

S. Acharya [126], D. Adamová [86], G. Aglieri Rinella [33], M. Agnello [30], N. Agrawal [51], Z. Ahammed [134], S. Ahmad[16], S.U. Ahn [71], I. Ahuja [38], A. Akindinov [142], M. Al-Turany [97], D. Aleksandrov [142], B. Alessandro [56], H.M. Alfanda [6], R. Alfaro Molina [67], B. Ali [16], A. Alici [26], N. Alizadehvandchali [115], A. Alkin [33], J. Alme [21], G. Alocco [52], T. Alt [64], A.R. Altamura [50], I. Altsybeev [95], M.N. Anaam [6], C. Andrei [46], N. Andreou [114], A. Andronic [137], V. Anguelov [94], F. Antinori [54], P. Antonioli [51], N. Apadula [74], L. Aphecetche [103], H. Appelshäuser [64], C. Arata [73], S. Arcelli [26], M. Aresti [23], R. Arnaldi [56], J.G.M.C.A. Arneiro [110], I.C. Arsene [20], M. Arslandok [139], A. Augustinus [33], R. Averbeck [97], M.D. Azmi[16], H. Baba[123], A. Badalà [53], J. Bae [104], Y.W. Baek [41], X. Bai [119], R. Bailhache [64], Y. Bailung [48], A. Balbino [30], A. Baldisseri [129], B. Balis [2], D. Banerjee [4], Z. Banoo [91], R. Barbera [27], F. Barile [32], L. Barioglio [95], M. Barlou[78], B. Barman[42], G.G. Barnaföldi [138], L.S. Barnby [85], V. Barret [126], L. Barreto [110], C. Bartels [118], K. Barth [33], E. Bartsch [64], N. Bastid [126], S. Basu [75], G. Batigne [103], D. Battistini [95], B. Batyunya [143], D. Bauri[47], J.L. Bazo Alba [101], I.G. Bearden [83], C. Beattie [139], P. Becht [97], D. Behera [48], I. Belikov [128], A.D.C. Bell Hechavarria [137], F. Bellini [26], R. Bellwied [115], S. Belokurova [142], Y.A.V. Beltran [45], G. Bencedi [138], S. Beole [25], Y. Berdnikov [142], A. Berdnikova [94], L. Bergmann [94], M.G. Besoiu [63], L. Betev [33], P.P. Bhaduri [134], A. Bhasin [91], M.A. Bhat [4], B. Bhattacharjee [42], L. Bianchi [25], N. Bianchi [49], J. Bielčík [36], J. Bielčíková [86], J. Biernat [107], A.P. Bigot [128], A. Bilandzic [95], G. Biro [138], S. Biswas [4], N. Bize [103], J.T. Blair [108], D. Blau [142], M.B. Blidaru [97], N. Bluhme[39], C. Blume [64], G. Boca [22,55], F. Bock [87], T. Bodova [21], A. Bogdanov[142], S. Boi [23], J. Bok [58], L. Boldizsár [138], M. Bombara [38], P.M. Bond [33], G. Bonomi [133,55], H. Borel [129], A. Borissov [142], A.G. Borquez Carcamo [94], H. Bossi [139], E. Botta [25], Y.E.M. Bouziani [64], L. Bratrud [64], P. Braun-Munzinger [97], M. Bregant [110], M. Broz [36], G.E. Bruno [96,32], M.D. Buckland [24], D. Budnikov [142], H. Buesching [64], S. Bufalino [30], P. Buhler [102], N. Burmasov [142], Z. Buthelezi [68,122], A. Bylinkin [21], S.A. Bysiak[107], M. Cai [6], H. Caines [139], A. Caliva [29], E. Calvo Villar [101], J.M.M. Camacho [109], P. Camerini [24], F.D.M. Canedo [110], M. Carabas [125], A.A. Carballo [33], F. Carnesecchi [33], R. Caron [127], L.A.D. Carvalho [110], J. Castillo Castellanos [129], F. Catalano [33,25], C. Ceballos Sanchez [143], I. Chakaberia [74], P. Chakraborty [47], S. Chandra [134], S. Chapeland [33], M. Chartier [118], S. Chattopadhyay [134], S. Chattopadhyay [99], T.G. Chavez [45], T. Cheng [97,6], C. Cheshkov [127], B. Cheynis [127], V. Chibante Barroso [33], D.D. Chinellato [111], E.S. Chizzali [I,95], J. Cho [58], S. Cho [58], P. Chochula [33], D. Choudhury[42], P. Christakoglou [84], C.H. Christensen [83], P. Christiansen [75], T. Chujo [124], M. Ciacco [30], C. Cicalo [52], F. Cindolo [51], M.R. Ciupek[97], G. Clai[II,51], F. Colamaria [50], J.S. Colburn[100], D. Colella [96,32], M. Colocci [26], M. Concas [III,33], G. Conesa Balbastre [73], Z. Conesa del Valle [130], G. Contin [24], J.G. Contreras [36], M.L. Coquet [129], P. Cortese [132,56], M.R. Cosentino [112], F. Costa [33], S. Costanza [22,55], C. Cot [130], J. Crkovská [94], P. Crochet [126], R. Cruz-Torres [74], P. Cui [6], A. Dainese [54], M.C. Danisch [94], A. Danu [63], P. Das [80], P. Das [4], S. Das [4], A.R. Dash [137], S. Dash [47], R.M.H. David[45], A. De Caro [29], G. de Cataldo [50], J. de Cuveland[39], A. De Falco [23], D. De Gruttola [29], N. De Marco [56], C. De Martin [24], S. De Pasquale [29], R. Deb [133], R. Del Grande [95], L. Dello Stritto [29], W. Deng [6], P. Dhankher [19], D. Di Bari [32], A. Di Mauro [33], B. Diab [129], R.A. Diaz [143,7], T. Dietel [113], Y. Ding [6], J. Ditzel [64], R. Divià [33], D.U. Dixit [19], Ø. Djuvsland[21], U. Dmitrieva [142], A. Dobrin [63], B. Dönigus [64], J.M. Dubinski [135], A. Dubla [97], S. Dudi [90], P. Dupieux [126], M. Durkac[106], N. Dzalaiova[13], T.M. Eder [137], R.J. Ehlers [74], F. Eisenhut [64], R. Ejima[92], D. Elia [50], B. Erazmus [103], F. Ercolessi [26], B. Espagnon [130], G. Eulisse [33], D. Evans [100], S. Evdokimov [142], L. Fabbietti [95], M. Faggin [28], J. Faivre [73], F. Fan [6], W. Fan [74], A. Fantoni [49], M. Fasel [87], A. Feliciello [56], G. Feofilov [142], A. Fernández Téllez [45], L. Ferrandi [110], M.B. Ferrer [33], A. Ferrero [129], C. Ferrero [56], A. Ferretti [25], V.J.G. Feuillard [94], V. Filova [36], D. Finogeev [142], F.M. Fionda [52], E. Flatland[33], F. Flor [115], A.N. Flores [108], S. Foertsch [68], I. Fokin [94], S. Fokin [142], E. Fragiacomo [57], E. Frajna [138], U. Fuchs [33], N. Funicello [29], C. Furget [73], A. Furs [142], T. Fusayasu [98], J.J. Gaardhøje [83], M. Gagliardi [25], A.M. Gago [101], T. Gahlaut[47], C.D. Galvan [109], D.R. Gangadharan [115], P. Ganoti [78], C. Garabatos [97], A.T. Garcia [130], J.R.A. Garcia [45], E. Garcia-Solis [9], C. Gargiulo [33], P. Gasik [97], A. Gautam [117], M.B. Gay Ducati [66], M. Germain [103], A. Ghimouz[124], C. Ghosh[134], M. Giacalone [51], G. Gioachin [30], P. Giubellino [97,56], P. Giubilato [28], A.M.C. Glaenzer [129], P. Glässel [94], E. Glimos [121], D.J.Q. Goh[76], V. Gonzalez [136], P. Gordeev[142], M. Gorgon [2], K. Goswami [48], S. Gotovac[34], V. Grabski [67], L.K. Graczykowski [135], E. Grecka [86], A. Grelli [59], C. Grigoras [33], V. Grigoriev [142], S. Grigoryan [143,1], F. Grosa [33], J.F. Grosse-Oetringhaus [33], R. Grosso [97], D. Grund [36], N.A. Grunwald[94], G.G. Guardiano [111], R. Guernane [73], M. Guilbaud [103], K. Gulbrandsen [83], T. Gündem [64], T. Gunji [123],

W. Guo [6], A. Gupta [91], R. Gupta [91], R. Gupta [48], S.P. Guzman [45], K. Gwizdziel [135], L. Gyulai [138], C. Hadjidakis [130], F.U. Haider [91], S. Haidlova [36], H. Hamagaki [76], A. Hamdi [74], Y. Han [140], B.G. Hanley [136], R. Hannigan [108], J. Hansen [75], M.R. Haque [135], J.W. Harris [139], A. Harton [9], H. Hassan [116], D. Hatzifotiadou [51], P. Hauer [43], L.B. Havener [139], S.T. Heckel [95], E. Hellbär [97], H. Helstrup [35], M. Hemmer [64], T. Herman [36], G. Herrera Corral [8], F. Herrmann[137], S. Herrmann [127], K.F. Hetland [35], B. Heybeck [64], H. Hillemanns [33], B. Hippolyte [128], F.W. Hoffmann [70], B. Hofman [59], G.H. Hong [140], M. Horst [95], A. Horzyk[2], Y. Hou [6], P. Hristov [33], C. Hughes [121], P. Huhn[64], L.M. Huhta [116], T.J. Humanic [88], A. Hutson [115], D. Hutter [39], R. Ilkaev[142], H. Ilyas [14], M. Inaba [124], G.M. Innocenti [33], M. Ippolitov [142], A. Isakov [84,86], T. Isidori [117], M.S. Islam [99], M. Ivanov [97], M. Ivanov[13], V. Ivanov [142], K.E. Iversen [75], M. Jablonski [2], B. Jacak [74], N. Jacazio [26], P.M. Jacobs [74], S. Jadlovska[106], J. Jadlovsky[106], S. Jaelani [82], C. Jahnke [110], M.J. Jakubowska [135], M.A. Janik [135], T. Janson[70], S. Ji [17], S. Jia [10], A.A.P. Jimenez [65], F. Jonas [87], D.M. Jones [118], J.M. Jowett [33,97], J. Jung [64], M. Jung [64], A. Junique [33], A. Jusko [100], M.J. Kabus [33,135], J. Kaewjai[105], P. Kalinak [60], A.S. Kalteyer [97], A. Kalweit [33], V. Kaplin [142], A. Karasu Uysal [72], D. Karatovic [89], O. Karavichev [142], T. Karavicheva [142], P. Karczmarczyk [135], E. Karpechev [142], U. Kebschull [70], R. Keidel [141], D.L.D. Keijdener[59], M. Keil [33], B. Ketzer [43], S.S. Khade [48], A.M. Khan [119], S. Khan [16], A. Khanzadeev [142], Y. Kharlov [142], A. Khatun [117], A. Khuntia [36], B. Kileng [35], B. Kim [104], C. Kim [17], D.J. Kim [116], E.J. Kim [69], J. Kim [140], J.S. Kim [41], J. Kim [58], J. Kim [69], M. Kim [19], S. Kim [18], T. Kim [140], K. Kimura [92], S. Kirsch [64], I. Kisel [39], S. Kiselev [142], A. Kisiel [135], J.P. Kitowski [2], J.L. Klay [5], J. Klein [33], S. Klein [74], C. Klein-Bösing [137], M. Kleiner [64], T. Klemenz [95], A. Kluge [33], A.G. Knospe [115], C. Kobdaj [105], T. Kollegger[97], A. Kondratyev [143], N. Kondratyeva [142], E. Kondratyuk [142], J. Konig [64], S.A. Konigstorfer [95], P.J. Konopka [33], G. Kornakov [135], M. Korwieser [95], S.D. Koryciak [2], A. Kotliarov [86], V. Kovalenko [142], M. Kowalski [107], V. Kozhuharov [37], I. Králik [60], A. Kravčáková [38], L. Krcal [33,39], M. Krivda [100,60], F. Krizek [86], K. Krizkova Gajdosova [33], M. Kroesen [94], M. Krüger [64], D.M. Krupova [36], E. Kryshen [142], V. Kučera [58], C. Kuhn [128], P.G. Kuijer [84], T. Kumaoka[124], D. Kumar[134], L. Kumar [90], N. Kumar[90], S. Kumar [32], S. Kundu [33], P. Kurashvili [79], A. Kurepin [142], A.B. Kurepin [142], A. Kuryakin [142], S. Kushpil [86], V. Kuskov[142], M.J. Kweon [58], Y. Kwon [140], S.L. La Pointe [39], P. La Rocca [27], A. Lakrathok[105], M. Lamanna [33], R. Langoy [120], P. Larionov [33], E. Laudi [33], L. Lautner [33,95], R. Lavicka [102], R. Lea [133,55], H. Lee [104], I. Legrand [46], G. Legras [137], J. Lehrbach [39], T.M. Lelek[2], R.C. Lemmon [85], I. León Monzón [109], M.M. Lesch [95], E.D. Lesser [19], P. Lévai [138], X. Li[10], J. Lien [120], R. Lietava [100], I. Likmeta [115], B. Lim [25], S.H. Lim [17], V. Lindenstruth [39], A. Lindner[46], C. Lippmann [97], D.H. Liu [6], J. Liu [118], G.S.S. Liveraro [111], I.M. Lofnes [21], C. Loizides [87], S. Lokos [107], J. Lomker [59], P. Loncar [34], X. Lopez [126], E. López Torres [7], P. Lu [97,119], F.V. Lugo [67], J.R. Luhder [137], M. Lunardon [28], G. Luparello [57], Y.G. Ma [40], M. Mager [33], A. Maire [128], M.V. Makariev [37], M. Malaev [142], G. Malfattore [26], N.M. Malik [91], Q.W. Malik[20], S.K. Malik [91], L. Malinina [VI,143], D. Mallick [130,80], N. Mallick [48], G. Mandaglio [31,53], S.K. Mandal [79], V. Manko [142], F. Manso [126], V. Manzari [50], Y. Mao [6], R.W. Marcjan [2], G.V. Margagliotti [24], A. Margotti [51], A. Marín [97], C. Markert [108], P. Martinengo [33], M.I. Martínez [45], G. Martínez García [103], M.P.P. Martins [110], S. Masciocchi [97], M. Masera [25], A. Masoni [52], L. Massacrier [130], O. Massen [59], A. Mastroserio [131,50], O. Matonoha [75], S. Mattiazzo [28], A. Matyja [107], C. Mayer [107], A.L. Mazuecos [33], F. Mazzaschi [25], M. Mazzilli [33], J.E. Mdhluli [122], Y. Melikyan [44], A. Menchaca-Rocha [67], J.E.M. Mendez [65], E. Meninno [102,29], A.S. Menon [115], M. Meres [13], S. Mhlanga[113,68], Y. Miake[124], L. Micheletti [33], D.L. Mihaylov [95], K. Mikhaylov [143,142], A.N. Mishra [138], D. Miśkowiec [97], A. Modak [4], B. Mohanty[80], M. Mohisin Khan[IV,16], M.A. Molander [44], S. Monira [135], C. Mordasini [116], D.A. Moreira De Godoy [137], I. Morozov [142], A. Morsch [33], T. Mrnjavac [33], V. Muccifora [49], S. Muhuri [134], J.D. Mulligan [74], A. Mulliri[23], M.G. Munhoz [110], R.H. Munzer [64], H. Murakami [123], S. Murray [113], L. Musa [33], J. Musinsky [60], J.W. Myrcha [135], B. Naik [122], A.I. Nambrath [19], B.K. Nandi [47], R. Nania [51], E. Nappi [50], A.F. Nassirpour [18], A. Nath [94], C. Nattrass [121], M.N. Naydenov [37], A. Neagu[20], A. Negru[125], E. Nekrasova[142], L. Nellen [65], R. Nepeivoda [75], S. Nese [20], G. Neskovic [39], N. Nicassio [50], B.S. Nielsen [83], E.G. Nielsen [83], S. Nikolaev [142], S. Nikulin [142], V. Nikulin [142], F. Noferini [51], S. Noh [12], P. Nomokonov [143], J. Norman [118], N. Novitzky [87], P. Nowakowski [135], A. Nyanin [142], J. Nystrand [21], M. Ogino [76], S. Oh [18], A. Ohlson [75], V.A. Okorokov [142], J. Oleniacz [135], A.C. Oliveira Da Silva [121], A. Onnerstad [116], C. Oppedisano [56], A. Ortiz Velasquez [65], J. Otwinowski [107], M. Oya[92], K. Oyama [76], Y. Pachmayer [94], S. Padhan [47], D. Pagano [133,55], G. Paić [65], A. Palasciano [50], S. Panebianco [129],

H. Park [124], H. Park [104], J. Park [58], J.E. Parkkila [33], Y. Patley [47], R.N. Patra[91], B. Paul [23], H. Pei [6], T. Peitzmann [59], X. Peng [11], M. Pennisi [25], S. Perciballi [25], D. Peresunko [142], G.M. Perez [7], Y. Pestov[142], V. Petrov [142], M. Petrovici [46], R.P. Pezzi [103,66], S. Piano [57], M. Pikna [13], P. Pillot [103], O. Pinazza [51,33], L. Pinsky[115], C. Pinto [95], S. Pisano [49], M. Płoskoń [74], M. Planinic[89], F. Pliquett[64], M.G. Poghosyan [87], B. Polichtchouk [142], S. Politano [30], N. Poljak [89], A. Pop [46], S. Porteboeuf-Houssais [126], V. Pozdniakov [143], I.Y. Pozos [45], K.K. Pradhan [48], S.K. Prasad [4], S. Prasad [48], R. Preghenella [51], F. Prino [56], C.A. Pruneau [136], I. Pshenichnov [142], M. Puccio [33], S. Pucillo [25], Z. Pugelova[106], S. Qiu [84], L. Quaglia [25], S. Ragoni [15], A. Rai [139], A. Rakotozafindrabe [129], L. Ramello [132,56], F. Rami [128], S.A.R. Ramirez [45], T.A. Rancien[73], M. Rasa [27], S.S. Räsänen [44], R. Rath [51], M.P. Rauch [21], I. Ravasenga [84], K.F. Read [87,121], C. Reckziegel [112], A.R. Redelbach [39], K. Redlich [V,79], C.A. Reetz [97], A. Rehman[21], F. Reidt [33], H.A. Reme-Ness [35], Z. Rescakova[38], K. Reygers [94], A. Riabov [142], V. Riabov [142], R. Ricci [29], M. Richter [20], A.A. Riedel [95], W. Riegler [33], A.G. Riffero [25], C. Ristea [63], M.V. Rodriguez [33], M. Rodríguez Cahuantzi [45], K. Røed [20], R. Rogalev [142], E. Rogochaya [143], T.S. Rogoschinski [64], D. Rohr [33], D. Röhrich [21], P.F. Rojas[45], S. Rojas Torres [36], P.S. Rokita [135], G. Romanenko [26], F. Ronchetti [49], A. Rosano [31,53], E.D. Rosas[65], K. Roslon [135], A. Rossi [54], A. Roy [48], S. Roy [47], N. Rubini [26], D. Ruggiano [135], R. Rui [24], P.G. Russek [2], R. Russo [84], A. Rustamov [81], E. Ryabinkin [142], Y. Ryabov [142], A. Rybicki [107], H. Rytkonen [116], J. Ryu [17], W. Rzesa [135], O.A.M. Saarimaki [44], S. Sadhu [32], S. Sadovsky [142], J. Saetre [21], K. Šafařík [36], P. Saha[42], S.K. Saha [4], S. Saha [80], B. Sahoo [47], B. Sahoo [48], R. Sahoo [48], S. Sahoo[61], D. Sahu [48], P.K. Sahu [61], J. Saini [134], K. Sajdakova[38], S. Sakai [124], M.P. Salvan [97], S. Sambyal [91], D. Samitz [102], I. Sanna [33,95], T.B. Saramela[110], P. Sarma [42], V. Sarritzu [23], V.M. Sarti [95], M.H.P. Sas [33], S. Sawan[80], J. Schambach [87], H.S. Scheid [64], C. Schiaua [46], R. Schicker [94], F. Schlepper [94], A. Schmah[97], C. Schmidt [97], H.R. Schmidt[93], M.O. Schmidt [33], M. Schmidt[93], N.V. Schmidt [87], A.R. Schmier [121], R. Schotter [128], A. Schröter [39], J. Schukraft [33], K. Schweda [97], G. Scioli [26], E. Scomparin [56], J.E. Seger [15], Y. Sekiguchi[123], D. Sekihata [123], M. Selina [84], I. Selyuzhenkov [97], S. Senyukov [128], J.J. Seo [94,58], D. Serebryakov [142], L. Šerkšnytė [95], A. Sevcenco [63], T.J. Shaba [68], A. Shabetai [103], R. Shahoyan[33], A. Shangaraev [142], A. Sharma[90], B. Sharma [91], D. Sharma [47], H. Sharma [54], M. Sharma [91], S. Sharma [76], S. Sharma [91], U. Sharma [91], A. Shatat [130], O. Sheibani[115], K. Shigaki [92], M. Shimomura[77], J. Shin[12], S. Shirinkin [142], Q. Shou [40], Y. Sibiriak [142], S. Siddhanta [52], T. Siemiarczuk [79], T.F. Silva [110], D. Silvermyr [75], T. Simantathammakul[105], R. Simeonov [37], B. Singh[91], B. Singh [95], K. Singh [48], R. Singh [80], R. Singh [91], R. Singh [48], S. Singh [16], V.K. Singh [134], V. Singhal [134], T. Sinha [99], B. Sitar [13], M. Sitta [132,56], T.B. Skaali[20], G. Skorodumovs [94], M. Slupecki [44], N. Smirnov [139], R.J.M. Snellings [59], E.H. Solheim [20], J. Song [17], C. Sonnabend [33,97], F. Soramel [28], A.B. Soto-hernandez [88], R. Spijkers [84], I. Sputowska [107], J. Staa [75], J. Stachel [94], I. Stan [63], P.J. Steffanic [121], S.F. Stiefelmaier [94], D. Stocco [103], I. Storehaug [20], P. Stratmann [137], S. Strazzi [26], A. Sturniolo [31,53], C.P. Stylianidis[84], A.A.P. Suaide [110], C. Suire [130], M. Sukhanov [142], M. Suljic [33], R. Sultanov [142], V. Sumberia [91], S. Sumowidagdo [82], S. Swain[61], I. Szarka [13], M. Szymkowski [135], S.F. Taghavi [95], G. Taillepied [97], J. Takahashi [111], G.J. Tambave [80], S. Tang [6], Z. Tang [119], J.D. Tapia Takaki [117], N. Tapus[125], L.A. Tarasovicova [137], M.G. Tarzila [46], G.F. Tassielli [32], A. Tauro [33], G. Tejeda Muñoz [45], A. Telesca [33], L. Terlizzi [25], C. Terrevoli [115], S. Thakur [4], D. Thomas [108], A. Tikhonov [142], N. Tiltmann [33,137], A.R. Timmins [115], M. Tkacik[106], T. Tkacik [106], A. Toia [64], R. Tokumoto[92], K. Tomohiro[92], N. Topilskaya [142], M. Toppi [49], T. Tork [130], P.V. Torres[65], V.V. Torres [103], A.G. Torres Ramos [32], A. Trifiró [31,53], A.S. Triolo [33,31,53], S. Tripathy [51], T. Tripathy [47], S. Trogolo [33], V. Trubnikov [3], W.H. Trzaska [116], T.P. Trzcinski [135], A. Tumkin [142], R. Turrisi [54], T.S. Tveter [20], K. Ullaland [21], B. Ulukutlu [95], A. Uras [127], G.L. Usai [23], M. Vala[38], N. Valle [22], L.V.R. van Doremalen[59], M. van Leeuwen [84], C.A. van Veen [94], R.J.G. van Weelden [84], P. Vande Vyvre [33], D. Varga [138], Z. Varga [138], M. Vasileiou [78], A. Vasiliev [142], O. Vázquez Doce [49], O. Vazquez Rueda [115], V. Vechernin [142], E. Vercellin [25], S. Vergara Limón[45], R. Verma[47], L. Vermunt [97], R. Vértesi [138], M. Verweij [59], L. Vickovic[34], Z. Vilakazi[122], O. Villalobos Baillie [100], A. Villani [24], A. Vinogradov [142], T. Virgili [29], M.M.O. Virta [116], V. Vislavicius[75], A. Vodopyanov [143], B. Volkel [33], M.A. Völkl [94], K. Voloshin[142], S.A. Voloshin [136], G. Volpe [32], B. von Haller [33], I. Vorobyev [95], N. Vozniuk [142], J. Vrláková [38], J. Wan[40], C. Wang [40], D. Wang[40], Y. Wang [40], Y. Wang [6], A. Wegrzynek [33], F.T. Weiglhofer[39], S.C. Wenzel [33], J.P. Wessels [137], S.L. Weyhmiller [139], J. Wiechula [64], J. Wikne [20], G. Wilk [79], J. Wilkinson [97], G.A. Willems [137], B. Windelband [94], M. Winn [129], J.R. Wright [108], W. Wu[40], Y. Wu [119], R. Xu [6], A. Yadav [43], A.K. Yadav [134],

S. Yalcin [72], Y. Yamaguchi [92], S. Yang[21], S. Yano [92], Z. Yin [6], I.-K. Yoo [17], J.H. Yoon [58], H. Yu[12], S. Yuan[21], A. Yuncu [94], V. Zaccolo [24], C. Zampolli [33], F. Zanone [94], N. Zardoshti [33], A. Zarochentsev [142], P. Závada [62], N. Zaviyalov[142], M. Zhalov [142], B. Zhang [6], C. Zhang [129], L. Zhang [40], S. Zhang [40], X. Zhang [6], Y. Zhang[119], Z. Zhang [6], M. Zhao [10], V. Zherebchevskii [142], Y. Zhi[10], D. Zhou [6], Y. Zhou [83], J. Zhu [97,6], Y. Zhu[6], S.C. Zugravel [56], N. Zurlo [133,55]

Affiliation Notes

[I] Also at: Max-Planck-Institut für Physik, Munich, Germany
[II] Also at: Italian National Agency for New Technologies, Energy and Sustainable Economic Development (ENEA), Bologna, Italy
[III] Also at: Dipartimento DET del Politecnico di Torino, Turin, Italy
[IV] Also at: Department of Applied Physics, Aligarh Muslim University, Aligarh, India
[V] Also at: Institute of Theoretical Physics, University of Wroclaw, Poland
[VI] Also at: An institution covered by a cooperation agreement with CERN

Collaboration Institutes

[1] A.I. Alikhanyan National Science Laboratory (Yerevan Physics Institute) Foundation, Yerevan, Armenia
[2] AGH University of Krakow, Cracow, Poland
[3] Bogolyubov Institute for Theoretical Physics, National Academy of Sciences of Ukraine, Kiev, Ukraine
[4] Bose Institute, Department of Physics and Centre for Astroparticle Physics and Space Science (CAPSS), Kolkata, India
[5] California Polytechnic State University, San Luis Obispo, California, United States
[6] Central China Normal University, Wuhan, China
[7] Centro de Aplicaciones Tecnológicas y Desarrollo Nuclear (CEADEN), Havana, Cuba
[8] Centro de Investigación y de Estudios Avanzados (CINVESTAV), Mexico City and Mérida, Mexico
[9] Chicago State University, Chicago, Illinois, United States
[10] China Institute of Atomic Energy, Beijing, China
[11] China University of Geosciences, Wuhan, China
[12] Chungbuk National University, Cheongju, Republic of Korea
[13] Comenius University Bratislava, Faculty of Mathematics, Physics and Informatics, Bratislava, Slovak Republic
[14] COMSATS University Islamabad, Islamabad, Pakistan
[15] Creighton University, Omaha, Nebraska, United States
[16] Department of Physics, Aligarh Muslim University, Aligarh, India
[17] Department of Physics, Pusan National University, Pusan, Republic of Korea
[18] Department of Physics, Sejong University, Seoul, Republic of Korea
[19] Department of Physics, University of California, Berkeley, California, United States
[20] Department of Physics, University of Oslo, Oslo, Norway
[21] Department of Physics and Technology, University of Bergen, Bergen, Norway
[22] Dipartimento di Fisica, Università di Pavia, Pavia, Italy
[23] Dipartimento di Fisica dell'Università and Sezione INFN, Cagliari, Italy
[24] Dipartimento di Fisica dell'Università and Sezione INFN, Trieste, Italy
[25] Dipartimento di Fisica dell'Università and Sezione INFN, Turin, Italy
[26] Dipartimento di Fisica e Astronomia dell'Università and Sezione INFN, Bologna, Italy
[27] Dipartimento di Fisica e Astronomia dell'Università and Sezione INFN, Catania, Italy
[28] Dipartimento di Fisica e Astronomia dell'Università and Sezione INFN, Padova, Italy
[29] Dipartimento di Fisica 'E.R. Caianiello' dell'Università and Gruppo Collegato INFN, Salerno, Italy
[30] Dipartimento DISAT del Politecnico and Sezione INFN, Turin, Italy
[31] Dipartimento di Scienze MIFT, Università di Messina, Messina, Italy
[32] Dipartimento Interateneo di Fisica 'M. Merlin' and Sezione INFN, Bari, Italy
[33] European Organization for Nuclear Research (CERN), Geneva, Switzerland
[34] Faculty of Electrical Engineering, Mechanical Engineering and Naval Architecture, University of Split, Split, Croatia
[35] Faculty of Engineering and Science, Western Norway University of Applied Sciences, Bergen, Norway

[36] Faculty of Nuclear Sciences and Physical Engineering, Czech Technical University in Prague, Prague, Czech Republic
[37] Faculty of Physics, Sofia University, Sofia, Bulgaria
[38] Faculty of Science, P.J. Šafárik University, Košice, Slovak Republic
[39] Frankfurt Institute for Advanced Studies, Johann Wolfgang Goethe-Universität Frankfurt, Frankfurt, Germany
[40] Fudan University, Shanghai, China
[41] Gangneung-Wonju National University, Gangneung, Republic of Korea
[42] Gauhati University, Department of Physics, Guwahati, India
[43] Helmholtz-Institut für Strahlen- und Kernphysik, Rheinische Friedrich-Wilhelms-Universität Bonn, Bonn, Germany
[44] Helsinki Institute of Physics (HIP), Helsinki, Finland
[45] High Energy Physics Group, Universidad Autónoma de Puebla, Puebla, Mexico
[46] Horia Hulubei National Institute of Physics and Nuclear Engineering, Bucharest, Romania
[47] Indian Institute of Technology Bombay (IIT), Mumbai, India
[48] Indian Institute of Technology Indore, Indore, India
[49] INFN, Laboratori Nazionali di Frascati, Frascati, Italy
[50] INFN, Sezione di Bari, Bari, Italy
[51] INFN, Sezione di Bologna, Bologna, Italy
[52] INFN, Sezione di Cagliari, Cagliari, Italy
[53] INFN, Sezione di Catania, Catania, Italy
[54] INFN, Sezione di Padova, Padova, Italy
[55] INFN, Sezione di Pavia, Pavia, Italy
[56] INFN, Sezione di Torino, Turin, Italy
[57] INFN, Sezione di Trieste, Trieste, Italy
[58] Inha University, Incheon, Republic of Korea
[59] Institute for Gravitational and Subatomic Physics (GRASP), Utrecht University/Nikhef, Utrecht, Netherlands
[60] Institute of Experimental Physics, Slovak Academy of Sciences, Košice, Slovak Republic
[61] Institute of Physics, Homi Bhabha National Institute, Bhubaneswar, India
[62] Institute of Physics of the Czech Academy of Sciences, Prague, Czech Republic
[63] Institute of Space Science (ISS), Bucharest, Romania
[64] Institut für Kernphysik, Johann Wolfgang Goethe-Universität Frankfurt, Frankfurt, Germany
[65] Instituto de Ciencias Nucleares, Universidad Nacional Autónoma de México, Mexico City, Mexico
[66] Instituto de Física, Universidade Federal do Rio Grande do Sul (UFRGS), Porto Alegre, Brazil
[67] Instituto de Física, Universidad Nacional Autónoma de México, Mexico City, Mexico
[68] iThemba LABS, National Research Foundation, Somerset West, South Africa
[69] Jeonbuk National University, Jeonju, Republic of Korea
[70] Johann-Wolfgang-Goethe Universität Frankfurt Institut für Informatik, Fachbereich Informatik und Mathematik, Frankfurt, Germany
[71] Korea Institute of Science and Technology Information, Daejeon, Republic of Korea
[72] KTO Karatay University, Konya, Turkey
[73] Laboratoire de Physique Subatomique et de Cosmologie, Université Grenoble-Alpes, CNRS-IN2P3, Grenoble, France
[74] Lawrence Berkeley National Laboratory, Berkeley, California, United States
[75] Lund University Department of Physics, Division of Particle Physics, Lund, Sweden
[76] Nagasaki Institute of Applied Science, Nagasaki, Japan
[77] Nara Women's University (NWU), Nara, Japan
[78] National and Kapodistrian University of Athens, School of Science, Department of Physics , Athens, Greece
[79] National Centre for Nuclear Research, Warsaw, Poland
[80] National Institute of Science Education and Research, Homi Bhabha National Institute, Jatni, India
[81] National Nuclear Research Center, Baku, Azerbaijan
[82] National Research and Innovation Agency - BRIN, Jakarta, Indonesia
[83] Niels Bohr Institute, University of Copenhagen, Copenhagen, Denmark
[84] Nikhef, National institute for subatomic physics, Amsterdam, Netherlands
[85] Nuclear Physics Group, STFC Daresbury Laboratory, Daresbury, United Kingdom
[86] Nuclear Physics Institute of the Czech Academy of Sciences, Husinec-Řež, Czech Republic
[87] Oak Ridge National Laboratory, Oak Ridge, Tennessee, United States

[88] Ohio State University, Columbus, Ohio, United States
[89] Physics department, Faculty of science, University of Zagreb, Zagreb, Croatia
[90] Physics Department, Panjab University, Chandigarh, India
[91] Physics Department, University of Jammu, Jammu, India
[92] Physics Program and International Institute for Sustainability with Knotted Chiral Meta Matter (SKCM2), Hiroshima University, Hiroshima, Japan
[93] Physikalisches Institut, Eberhard-Karls-Universität Tübingen, Tübingen, Germany
[94] Physikalisches Institut, Ruprecht-Karls-Universität Heidelberg, Heidelberg, Germany
[95] Physik Department, Technische Universität München, Munich, Germany
[96] Politecnico di Bari and Sezione INFN, Bari, Italy
[97] Research Division and ExtreMe Matter Institute EMMI, GSI Helmholtzzentrum für Schwerionenforschung GmbH, Darmstadt, Germany
[98] Saga University, Saga, Japan
[99] Saha Institute of Nuclear Physics, Homi Bhabha National Institute, Kolkata, India
[100] School of Physics and Astronomy, University of Birmingham, Birmingham, United Kingdom
[101] Sección Física, Departamento de Ciencias, Pontificia Universidad Católica del Perú, Lima, Peru
[102] Stefan Meyer Institut für Subatomare Physik (SMI), Vienna, Austria
[103] SUBATECH, IMT Atlantique, Nantes Université, CNRS-IN2P3, Nantes, France
[104] Sungkyunkwan University, Suwon City, Republic of Korea
[105] Suranaree University of Technology, Nakhon Ratchasima, Thailand
[106] Technical University of Košice, Košice, Slovak Republic
[107] The Henryk Niewodniczanski Institute of Nuclear Physics, Polish Academy of Sciences, Cracow, Poland
[108] The University of Texas at Austin, Austin, Texas, United States
[109] Universidad Autónoma de Sinaloa, Culiacán, Mexico
[110] Universidade de São Paulo (USP), São Paulo, Brazil
[111] Universidade Estadual de Campinas (UNICAMP), Campinas, Brazil
[112] Universidade Federal do ABC, Santo Andre, Brazil
[113] University of Cape Town, Cape Town, South Africa
[114] University of Derby, Derby, United Kingdom
[115] University of Houston, Houston, Texas, United States
[116] University of Jyväskylä, Jyväskylä, Finland
[117] University of Kansas, Lawrence, Kansas, United States
[118] University of Liverpool, Liverpool, United Kingdom
[119] University of Science and Technology of China, Hefei, China
[120] University of South-Eastern Norway, Kongsberg, Norway
[121] University of Tennessee, Knoxville, Tennessee, United States
[122] University of the Witwatersrand, Johannesburg, South Africa
[123] University of Tokyo, Tokyo, Japan
[124] University of Tsukuba, Tsukuba, Japan
[125] University Politehnica of Bucharest, Bucharest, Romania
[126] Université Clermont Auvergne, CNRS/IN2P3, LPC, Clermont-Ferrand, France
[127] Université de Lyon, CNRS/IN2P3, Institut de Physique des 2 Infinis de Lyon, Lyon, France
[128] Université de Strasbourg, CNRS, IPHC UMR 7178, F-67000 Strasbourg, France, Strasbourg, France
[129] Université Paris-Saclay, Centre d'Etudes de Saclay (CEA), IRFU, Départment de Physique Nucléaire (DPhN), Saclay, France
[130] Université Paris-Saclay, CNRS/IN2P3, IJCLab, Orsay, France
[131] Università degli Studi di Foggia, Foggia, Italy
[132] Università del Piemonte Orientale, Vercelli, Italy
[133] Università di Brescia, Brescia, Italy
[134] Variable Energy Cyclotron Centre, Homi Bhabha National Institute, Kolkata, India
[135] Warsaw University of Technology, Warsaw, Poland
[136] Wayne State University, Detroit, Michigan, United States
[137] Westfälische Wilhelms-Universität Münster, Institut für Kernphysik, Münster, Germany
[138] Wigner Research Centre for Physics, Budapest, Hungary
[139] Yale University, New Haven, Connecticut, United States
[140] Yonsei University, Seoul, Republic of Korea

[141] Zentrum für Technologie und Transfer (ZTT), Worms, Germany
[142] Affiliated with an institute covered by a cooperation agreement with CERN
[143] Affiliated with an international laboratory covered by a cooperation agreement with CERN.